LOPINAVIR CONCEPT ARTICLE

Prepared for submission to Journal of Non-Crystalline Solids

Preparation and evaluation of metastable forms of lopinavir

H. J. R. Lemmer*, N. Stieger, W. Liebenberg

Unit for Drug Research and Development, Faculty of Health Sciences, North-West University, Potchefstroom, South Africa

* Corresponding author: H.J.R. Lemmer
Tel: +27 (018) 299 4015
Fax: +27 (018) 293 5219
E-mail address: Righard.Lemmer@nwu.ac.za
Postal address: Internal Box 36, Private Bag X6001, Potchefstroom, 2520

Abstract

In this work, we present the preparation and evaluation of previously unreported metastable forms of the antiretroviral drug, lopinavir. Lopinavir possesses significant structural flexibility and capacity for extensive hydrogen bonding – factors that enable a compound to present a multitude of stable and metastable structural states. By maintaining the chemical structure, physicochemical properties like the glass transition temperature (T_g), dissolution and solubility can readily be attributed to the structural stability of the system. Commercially-available lopinavir was used to prepare partially amorphous crystals, semicrystalline needles, resins and glasses. The physicochemical properties of each were investigated using differential scanning calorimetry (DSC), Fourier transform infrared spectroscopy (FTIR) and powder X-ray diffraction (PXRD). Each sample's thermal and spectroscopic analyses, as well as dissolution and solubility studies were performed one month after preparation of said sample, to increase comparability. Glass transition temperature, activation energy for global molecular mobility (ΔE_{Tg}), and activation energy for local molecular mobility (ΔE_{β}) were assessed as primary indicators for structural stability of the systems. Relating these properties to aqueous solubility revealed that each metastable form possessed its own unique equilibrium solubility. Normalised cumulative dissolved fractions (α) were fitted against deceleratory kinetics models, and from the data hereby obtained the dissolution process was determined to followed first-order kinetics ($R^2 = 0.998$). From the rate constants, the activation energy for dissolution (ΔE_{Diss}) of each sample was calculated. Interestingly, the ΔE_{Diss} values of the samples analysed appeared to correlate with the ΔE_{β} values of said metastable forms, however, further investigation will be required before drawing any conclusions from this potential correlation.

Keywords Metastable, lopinavir, physicochemical evaluation, dissolution, solubility

1 Introduction

Lopinavir is a peptidomimetic antiretroviral (ARV) agent which inhibits the human immunodeficiency virus (HIV) protease enzyme from cleaving the Gag-Pol polyprotein, resulting in the production of immature, non-infectious viral particles [1]. Its chemical structure is flexible, with 4 chiral centres, and possesses the potential to undergo extensive inter- and intramolecular hydrogen bonding. This structural flexibility renders lopinavir susceptible to adopting numerous molecular coordinates on its energy landscape, increasing the probability of preparing various amorphous and crystalline forms [2]. The peptidomimetic structure of lopinavir also imparts an unfavourable pharmacokinetic profile on the drug due to low aqueous solubility, poor absorption and rapid hepatobiliary elimination [3]. To address the hepatobiliary elimination, ritonavir is co-administered with lopinavir to outcompete its elimination. The poor solubility of lopinavir can be addressed by preparing amorphous forms of the drug. The high internal energy and specific volume of the amorphous state have already been reported to enhance dissolution, solubility and bioavailability [4,5]. However, amorphous material is known to be inherently unstable, and will eventually crystallise into a lower energy state.

To date, the glass transition temperature (T_g) and its role with regards to formulation, storage, nucleation and crystal growth, used to be the mainstay parameter for assessing the stability of amorphous systems [6-10]. However, in several instances the T_g failed to be an accurate indicator of stability [11-13]. Recently, local molecular motions (β-relaxations) have been recognized as an important determinant of the stability of amorphous systems, not only with regards to coupling with global molecular motions (α-relaxations), but also concerning crystallization well below and close to T_g, as well as the aggregation of macromolecules [11,14-19]. An added advantage of evaluating β-relaxations to determine the stability of amorphous systems, is that it allows investigation of the effects of low temperature and low energy disturbances on the system. The energy barrier imposed by the activation energy for β-relaxation (ΔE_β) can therefore be seen as the first step in re-establishing the energetic equilibrium of molecular mobility in amorphous systems under stress conditions, such as heating.

Studies on amorphous material usually consist of the preparation of an amorphous sample from a fully crystalline material, usually via ball milling, spray drying or cooling of the melt, followed by a comparison of the physicochemical properties of the newly formed amorphous sample to that of the original crystalline material. In this study, commercial lopinavir was recrystallized from various organic solvents to yield amorphous resins and partially amorphous crystals. In keeping with the norm for studies on amorphous material, two glasses were also prepared from the melt. One was quench cooled with liquid nitrogen and the other was cooled under ambient temperature to yield glasses with

different degrees of disorder [2,20.21]. To thoroughly evaluate the stability of each system, both α- and β-relaxations were investigated. The glasses, recrystallisation products and commercial lopinavir were thermally analysed to determine the ΔE_{β}, fragility (m) and strength (D) parameters. These parameters were then correlated with solubility data to investigate their relations. Dissolution data were fitted to deceleratory kinetics models, and from this data the activation energy for dissolution (ΔE_{Diss}) were obtained. The rationale behind fitting the data to these models was to relate dissolution to changes on the surfaces of the solid particles, since dissolution under sink conditions in effect reverses crystallisation by removing solute molecules from the surface of the solid phase. To maintain uniformity, all sample analyses were carried out one month after the preparation of the specific sample.

2 Materials and Methods

2.1 Materials

Lopinavir (HPLC assay > 99%) was purchased from Dr, Reddy's Laboratories Ltd., Andhra Pradesh, India.

2.2 Methods

Differential Scanning Calorimetry (DSC). DSC experiments were carried out on a Shimadzu DSC-60A (Shimadzu, Japan). The DSC cell was purged with nitrogen at 35 mL/min. Indium and tin standards were used to calibrate the temperature and heat of fusion. All samples were accurately weighed (5 – 6 mg) and analysed in aluminium pans with pierced lids to facilitate potential volatile evolution during heating. The data was analysed using ta60 software version 2.11.

To investigate β-relaxations, the optimum annealing conditions were found to be an annealing time of 20 minutes at a temperature of 0.8 T_g, consistent with known literature [22]. Because of the inherently small endothermic peaks associated with β-relaxations, heating rates of 10, 15 and 20 K/min were used. Scanning rates < 10 K/min displayed oscillation between enthalpy loss and recovery, rendering accurate data collection difficult and rates > 20 K/min lead to overlap of the β and α-processes. To investigate α-relaxations, the samples were annealed for 10 minutes at temperatures 20 K above T_g [23]. The samples were analysed at heating rates of 5, 10 and 20 K. For both the β and α-relaxations similar cooling and reheating rates were maintained [24,25]. To maintain uniformity, all sample analyses were carried out one month after the preparation of the specific sample.

The activation energies for local and global molecular mobility were calculated from non-isothermal DSC data using Equation 1 [22,23].

$$\frac{-\Delta E_a}{R} = \frac{d(\ln q)}{d(T_g^{-1})} \quad (1)$$

Where the activation energy (ΔE_a) can be written as ΔE_β, for local relaxations, and ΔE_{Tg} for global relaxations. From ΔE_{Tg} the m values were calculated (Equation 2) [23].

$$m = \frac{\Delta E_{Tg}}{(\ln 10) R T_g} \quad (2)$$

The minimum value of m (m_{min}) was determined to be 16, and from that the D value of each sample was calculated (Equation 3) [23].

$$D = \frac{(\ln 10) m_{\min}^{\ 2}}{(m - m_{\min})} \quad (3)$$

Thermogravimetric Analysis (TGA). TGA experiments were performed using a Shimadzu DTG-60 (Shimadzu, Japan). The TGA chamber was purged with nitrogen at 35 mL/min. Indium and tin standards were used to calibrate the temperature. All samples were accurately weighed (7 – 8 mg) and analysed in open aluminium pans. The data was analyzed using ta60 software version 2.11.

Fourier Transform Infrared Spectroscopy (FTIR). FTIR analyses were performed using a Shimadzu IRPrestige-21 (Shimadzu, Japan). Peak positions were confirmed using polystyrene film. Spectra were recorded over a range of 500 – 4000 cm^{-1}. All samples were accurately weighed (4 – 5 mg) and homogeneously dispersed in a ground matrix of KBr. The data was analysed using Shimadzu IRsolution software version 1.40.

Ultraviolet-Visible Absorption Spectrophotometry (UV-vis). UV-vis analyses were carried out on a Shimadzu UV-1800 (Shimadzu, Japan). Analyses were conducted at 210 nm in quartz cuvettes using Shimadzu UVProbe software version 2.32.

Hot stage microscopy. Hot stage micrographs were taken on a Nikon Eclipse E400 microscope (Nikon, Japan) equipped with a Nikon DS-Fi1 camera and cross-polarised light filter. Images were acquired with NIS-Elements software version 3.22.

Powder X-Ray Diffraction (PXRD). PXRD analyses were carried out on a PANalytical X'Pert Pro (PANalytical, Netherlands). Measurement conditions were: Anode, Cu; Kα_1, 1.5405 Å; Kα_2, 1.54443 Å; K-Beta, 1.39225 Å; Kα_1/Kα_2 ratio, 0.5; Generator settings, 40 mA, 45 kV; divergence slit, 0.957°, fixed; step size, 0.017° in 2θ; scan step times, 19.685 s; temperature, 25 °C. The data was analyzed using X'Pert Data Collector software version 4.0A.

Solubility. Aqueous solubility of each sample was determined by stirring a supersaturated solution of each prepared material at 310 K for 24 hours to reach equilibrium solubility. Concentrations were determined by measuring the UV-vis absorbance. Linearity was observed in the range 0.01 to 200 μg/mL.

Dissolution. To control the particle size distribution, samples were sieved and the fraction between 400 – 1400 μm collected. Accurately weighed (54 – 56 mg) amounts of these samples were dissolved in 10 mL double distilled water at 298, 308 and 318 K over 4 hours. Withdrawals were made at 1 minute intervals for the first 5 minutes, and then at longer intervals and analyzed by UV-vis absorbance.

Normalised cumulative dissolved fractions (α) were fitted against deceleratory solid-state kinetic models (Table 1) and the rate constants (k) thereby obtained were used to determine the activation energy of dissolution (ΔE_{Diss}) for each sample using the well-known Arrhenius equation (Equation 6).

$$k = Ae^{-\left(\frac{\Delta E_{Diss}}{RT}\right)} \quad (6)$$

Where A is the frequency factor and R the gas constant.

3 Results

Recrystallisation of lopinavir yielded crystals from acetone and ethyl acetate, semicrystalline needles from diethyl ether and resins from chloroform and dichloromethane. Two glasses were also prepared from the melt. One was quenched with liquid nitrogen (henceforth referred to as QG) and the other was allowed to cool at ambient temperature (AG). Thermal analyses indicated that commercial lopinavir is amorphous, and even the crystals obtained from acetone and ethyl acetate contained some amorphous material (Figure 1). The resin obtained from chloroform also exhibited a melting endotherm, suggesting the presence of crystallites in the amorphous matrix. The results from the DSC analyses concerning crystalline content were corroborated by PXRD data (Figure 2). Both the glasses as well as the resin obtained from dichloromethane displayed only diffuse halo bands on their PXRD diffractograms (supplementary information, Figure S13).

Unfortunately, the exact crystalline content, usually determined using the methods described by Lefort et al. [26] and Black and Lovering [27], could not be reliably applied in this in this study, because of the absence of a 100 % crystalline sample. However, birefringence could still be used to visualise the crystallites present in the more amorphous samples, e.g. the resin from chloroform and the glasses obtained from cooling of the melt (Figure 3).

Results from the β-relaxation and fragility studies are presented in Table 2. The extremely fragile behaviour observed for the lopinavir crystals from acetone and ethyl acetate can be attributed to their small amounts of amorphous content (Figure 1 and 2). Due to their small size, these amorphous regions undergo rapid changes at T_β and T_g, increasing the slopes of their Arrhenius plots, and therefore the activation energy, resulting in unusually high values of ΔE when compared to other lopinavir samples (supplementary information, Figures S18 to S21). This could probably be remedied by increasing the sample size, however sufficient increase would have required samples larger than what could be contained in a DSC crucible.

The differences in crystalline content, as seen from the PXRD data (Figures 2 and S13), between the lopinavir resins prepared in this study can also be elucidated by their differences in ΔE_β (Table 2). The gum-like properties of a resin, coupled with its long setting time, offer significantly more freedom for molecular motion than a glass or crystal. In resins, local regions with energies exceeding that of ΔE_β can offer sufficient molecular mobility for nucleation to occur, leading to the random distribution of crystallites observed in the resin from chloroform (Figure 3). Commercial lopinavir displayed the highest ΔE_β of all the amorphous samples, explaining its stability and resistance to crystallisation following short term energy changes, e.g. shipping, handling and storage for extended periods of time at temperatures below T_g.

AG exhibited the highest aqueous solubility (see Table 3), followed by the resin obtained from chloroform, while other predominantly amorphous samples, e.g. QG and the resin obtained from dichloromethane, displayed solubility values only slightly higher than those of the crystalline samples. As expected, the predominantly amorphous lopinavir samples were more soluble than their more crystalline counterparts. However, there was no clear cut correlation between solubility and ΔE_{Tg}. Only ΔE_β appeared to correlate with solubility, albeit inversely.

Based on their physical properties, the crystals from ethyl acetate, QG and AG were chosen for dissolution studies. These samples shared the ability to be broken, without being totally crushed, and sieved to obtain a similar size distribution of each sample, thereby eliminating yet another variable that could account for differences in dissolution rate. By maintaining the chemical structure, particle size distribution, analysis temperature, stirring rate and dissolution medium, differences in dissolution rate can more readily be ascribed to the metastability of the sample in question. The dissolved concentrations were expressed as normalised cumulative dissolved fractions (α) and straight line regions of the curves (Figure 5), consisting of α values ranging from 0.1 to 0.8, were fitted against deceleratory solid-state kinetics models presented in Table 1 (for further information, see supplementary information, Figures S22 to S24). These straight line regions represent dissolution under sink conditions. Results from the model fitting indicated that the dissolution process followed

first-order kinetics (R^2 = 0.998). From the dissolution rate constants, the ΔE_{Diss} for the lopinavir crystals, QG and AG were determined as 36, 22 and 18 kJ/mol respectively.

4 Discussion

As expected, the inherent structural flexibility of lopinavir and its capacity to undergo extensive hydrogen bonding led to a solid-state structure presenting a wide range of metastable forms with varying degrees of molecular mobility and amorphous content. A physicochemical analysis of lopinavir, its glasses and recrystallisation products was undertaken to obtain several parameters which are known to influence the stability of a system, e.g. ΔE_{Tg}, the most commonly used parameter for assessing the stability of an amorphous system. During the course of the analyses, several incidents where stability would have been wrongfully assigned if only considering ΔE_{Tg} became clear, e.g. commercial lopinavir would have been dubbed the second most unstable lopinavir sample (ΔE_{Tg} 144 kJ/mol). However, it is stable for extended periods of time and is resistant to crystallisation following handling, while the resin obtained from chloroform displayed a ΔE_{Tg} of 203 kJ/mol and formed large amounts of crystallites in its amorphous matrix even while stored well below T_g. In both these cases the true physical stability could be deduced from ΔE_{β} (see Table 2).

Relating the solubility data to the physicochemical parameters obtained from thermal analyses gave the well known trend in which the solubility increases when moving from crystalline to amorphous systems. However, amongst the amorphous samples the solubility did not increase with increasing amorphous content (Figure 4). The best correlation was found between solubility and ΔE_{β}. Interestingly, the ΔE_{Diss} values of the lopinavir samples analysed exhibited the same trend as their respective ΔE_{β} values, suggesting that the lower activation energy barrier imposed by lower values of ΔE_{β} might facilitate the removal of molecules from the solid's surface, thereby decreasing the amount of energy needed to dissolve a sample and increasing the dissolution rate. However, extensive future studies will have to be carried out before drawing any conclusions from this potential correlation between ΔE_{β} and ΔE_{Diss}.

5 Conclusion

In this work we illustrated the ability of a chemical species to rearrange into several metastable forms, depending on the preparation conditions, as well as the need to perform a thorough physical chemical screening in order to obtain a full picture of the stability of a system. Combining several analytical techniques and methods to evaluate the systems, made it clear that each of these metastable forms displayed its own unique physicochemical behaviour and stability. The knowledge obtained from this study can assist in future research and formulation of lopinavir and similar peptidomimetic drugs.

6 Acknowledgement

The authors thank the North-West University and the National Research Foundation (NRF) of South Africa for funding this work.

Figures

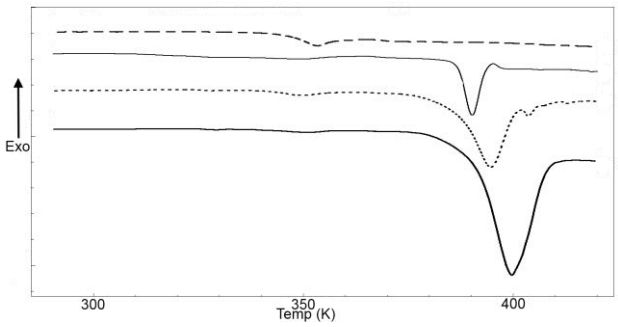

Figure 1 DSC curves of commercial lopinavir (dashed), lopinavir resin from chloroform (thin solid), lopinavir crystals from ethyl acetate (dotted) and acetone (thick solid). Thermograms were obtained from heating at 10 K/min.

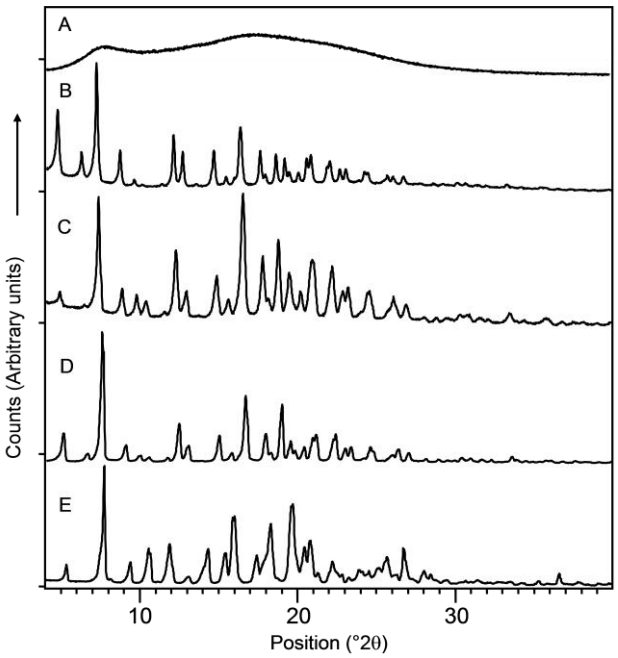

Figure 2 PXRD diffractograms of commercial lopinavir (A), needles from diethyl ether (B), resin from chloroform (C) and crystals from ethyl acetate (D) and acetone (E).

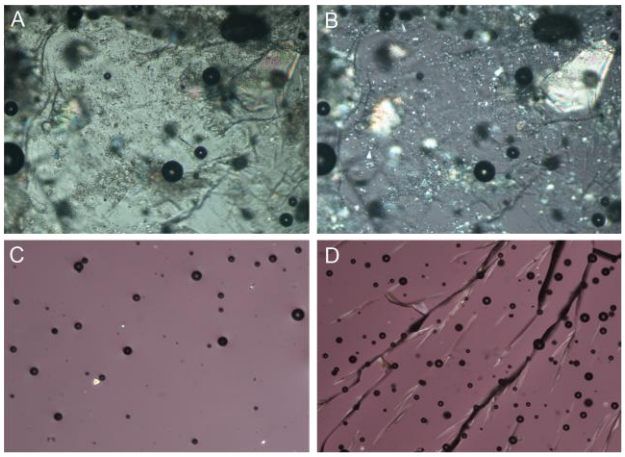

Figure 3 Micrograms of lopinavir resin from chloroform (A and B), AG (C) and QG (D), where birefringence was used in B, C and D to visualize the crystallites embedded in the amorphous matrixes.

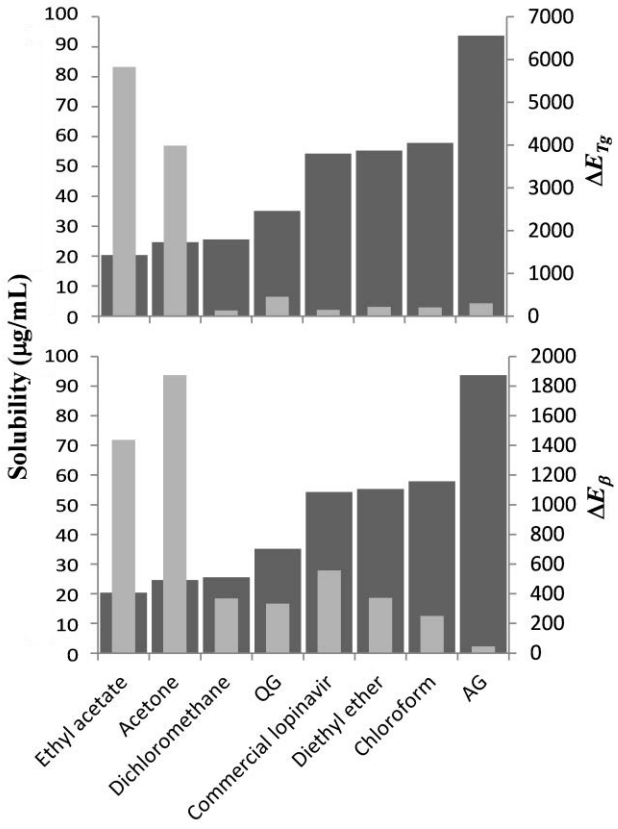

Figure 4 Correlation between solubility (primary y-axis, dark grey) and τ_{DSC}, ΔE_{Tg} and ΔE_{β} (secondary y-axis, light grey) respectively.

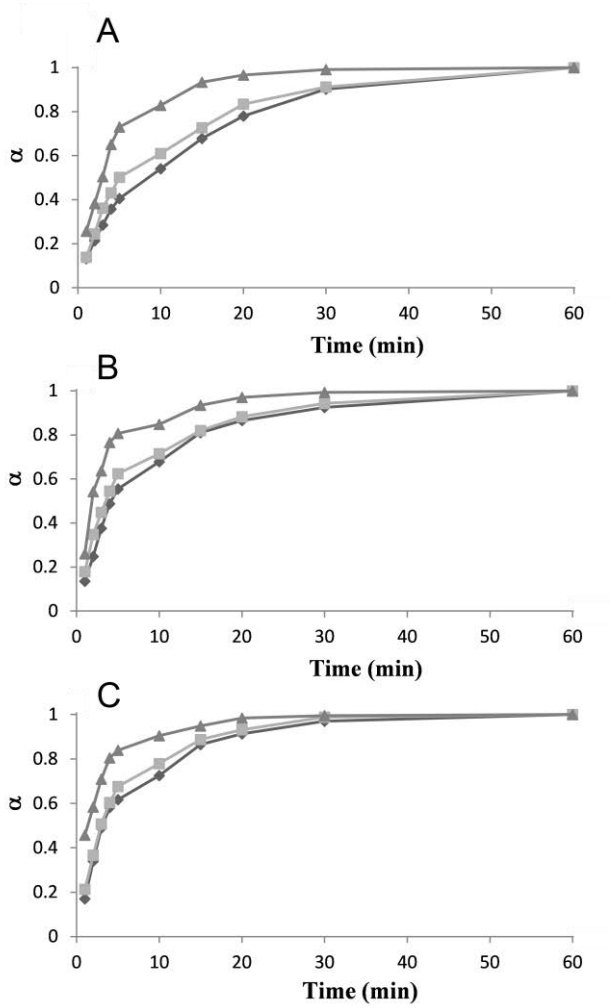

Figure 5 Dissolution curves of lopinavir crystals from ethyl acetate (A), QG (B) and AG (C) at 298 K (diamonds), 308 K (squares) and 318 K (triangles).

Tables

Table 1 Rate equations of deceleratory kinetic models [28]

Model	Integral form $g(\alpha) = kt$
Sigmoid rate equations	
Avarami-Erofe'ev (A2)	$[-\ln(1 - \alpha)]^{1/2}$
Avarami-Erofe'ev (A3)	$[-\ln(1 - \alpha)]^{1/3}$
Avarami-Erofe'ev (A4)	$[-\ln(1 - \alpha)]^{1/4}$
Diffusion models	
One-dimensional diffusion (D1)	α^2
Two-dimensional diffusion (D2)	$[(1 - \alpha)\ln(1 - \alpha)] + \alpha$
Three-dimensional diffusion (D3)	$[1 – (1 - \alpha)^{1/3}]^2$
Ginstling-Brounshtein (D4)	$1 – (2\alpha/3) – (1 - \alpha)^{2/3}$
Reaction-order models	
First-order (F1)	$-\ln(1 - \alpha)$
Second-order (F2)	$(1 - \alpha)^{-1} – 1$
Third-order (F3)	$0.5((1 - \alpha)^{-2} – 1)$

Table 2 Values of T_β and T_g when heated at 10 K/min (mean ± S.D.), activation energies for β- and α-processes and the fragility (m) and strength (D) parameters of each sample

Preparation conditions	T_β(K)	T_g (K)	ΔE (kJ/mol)					
	10 K/min	10 K/min	T_β	T_β^{mid}	T_g	T_g^{mid}	m	D
Lopinavir	330 ± 1.56	348 ± 0.41	557	325	144	140	21	106
Ethyl acetate	331 ± 0.23	346 ± 0.67	1438	524	5831	595	880	1
Acetone	331 ± 1.24	350 ± 0.06	1873	671	3989	1979	561	1
Diethyl ether	329 ± 0.17	340 ± 2.36	372	251	217	126	33	34
Chloroform	329 ± 1.64	339 ± 2.82	250	211	203	165	31	39
Dichloromethane	329 ± 1.72	331 ± 6.61	368	294	133	94	20	130
AG	301 ± 1.04	318 ± 0.08	45	26	302	340	50	17
QG	318 ± 0.66	351 ± 0.39	334	273	453	275	67	11

Table 3 Aqueous solubility (mean ± S.D.) of commercial lopinavir, its glasses and recrystallisation products

Preparation conditions	Solubility (μg/mL)
Commercial lopinavir	54.3 ± 0.7
Ethyl acetate	20.4 ± 0.7
Acetone	24.7 ± 0.6
Diethyl ether	55.3 ± 0.4
Chloroform	57.9 ± 0.9
Dichloromethane	25.6 ± 0.2
AG	93.7 ± 0.9
QG	35.2 ± 0.6

References

[1] S. Safrin, in: B.G. Katzung (Ed.), Basic and Clinical Pharmacology, McGraw-Hill, Singapore, 2004, pp 801-827.

[2] F.H. Stillinger, Science, 267 (1995) 1935-1939.

[3] D.J. Kempf, K.C. Marsh, G. Kumar, A.D. Rodrigues, J.F. Denissen, E. McDonald, M.J. Kukulka, A. Hsu, G.R. Granneman, P.A. Baroldi, E. Sun, D. Pizzuti, J.J. Plattner, D.W. Norbeck, J.M. Leonard, Antimicrob. Agents Chemother. 41 (1997) 654-660.

[4] B.C. Hancock, M. Parks, Pharm. Res. 17 (2000) 397-404.

[5] R. Hüttenrauch, Acta Pharm. Technol., Suppl. 6 (1978) 55-127.

[6] A.A. Elamin, G. Alderborn, C. Ahlneck, Int. J. Pharm. 108 (1994) 213-224.

[7] H. Levine, L. Slade, J. Chem. Soc., Faraday Trans. 1, 84 (1988) 2619-2633.

[8] N. Lordi, P. Shiromani, Drug Dev. Ind. Pharm. 10 (1984) 729-752.

[9] A.G. Mitchell, G.R.B. Down, Int. J. Pharm. 22 (1984) 337-344.

[10] G.H. Ward, R.K. Schultz, Pharm. Res. 12 (1995) 773-779.

[11] S. Vyazovkin, I. Dranca, J. Phys. Chem. B, 111 (2007) 7283-7287.

[12] S. Yoshioka, T. Miyazaki, Y. Aso, Pharm. Res. 23 (2006) 961-966.

[13] S. Yoshioka, T. Miyazaki, Y. Aso, T. Kawanishi, Pharm. Res. 24 (2007) 1660-1667.

[14] J. Alie, J. Menegotto, P. Cardon, H. Duplaa, A. Caron, C. Lacabanne, M. Bauer, J. Pharm. Sci. 93 (2004) 218-233.

[15] I. Alig, D. Braun, R. Langendorf, M. Voigt, J.H. Wendorff, J. Non-Cryst. Solids, 221 (1997) 261-264.

[16] C. Bhugra, R.A. Shmeis, S.L. Krill, M.J. Pikal, J. Pharm. Sci. 97 (2007) 455-472.

[17] T. Hikima, M. Hanaya, M. Oguni, J. Mol. Struct. 479 (1999) 245-250.

[18] K.L. Ngai, J. Phys.: Condens. Matter, 14 (2003) S1107-S1125.

[19] S. Vyazovkin, I. Dranca, J. Phys. Chem. B, 109 (2005) 18637-18644.

[20] S. Aasland, P.F. McMillan, Nature, 369 (1994) 633-636.

[21] M.D. Ediger, Annu. Rev. Phys. Chem. 51 (2000) 99-128.

[22] S. Vyazovkin, I. Dranca, Pharm. Res. 23 (2006) 422-428.

[23] K.J. Crowley, G. Zografi, Thermochim. Acta, 380 (2001) 79-93.

[24] S.N. Crichton, C.T. Moynihan, J. Non-Cryst. Solids, 99 (1988) 413-417.

[25] C.T. Moynihan, A.J. Easteal, J. Wilder, J. Tucker, J. Phys. Chem. 78 (1974) 2673-2677.

[26] R. Lefort, A. Gusseme, F.-J. Willart, F. Danède, M. Descamps, Int. J. Pharm. 280 (2004) 209-219.

[27] D.B. Black, E.G. Lovering, J. Pharm. Pharmacol. 29 (1977) 684-687.

[28] W.E. Brown, D. Dollimore, A.K. Galwey, in: C.H. Bamford, C.F.H Tipper, (Eds.), Comprehensive Chemical Kinetics, vol. 22, Elsevier, Amsterdam, 1980, pp 41-113.

Preparation and evaluation of metastable forms of lopinavir

H. J. R. Lemmer*, N. Stieger, W. Liebenberg

Unit for Drug Research and Development, Faculty of Health Sciences, North-West University, Potchefstroom, South Africa

Supplementary Information

In this section, commercial lopinavir will be referred to as lopinavir raw material.

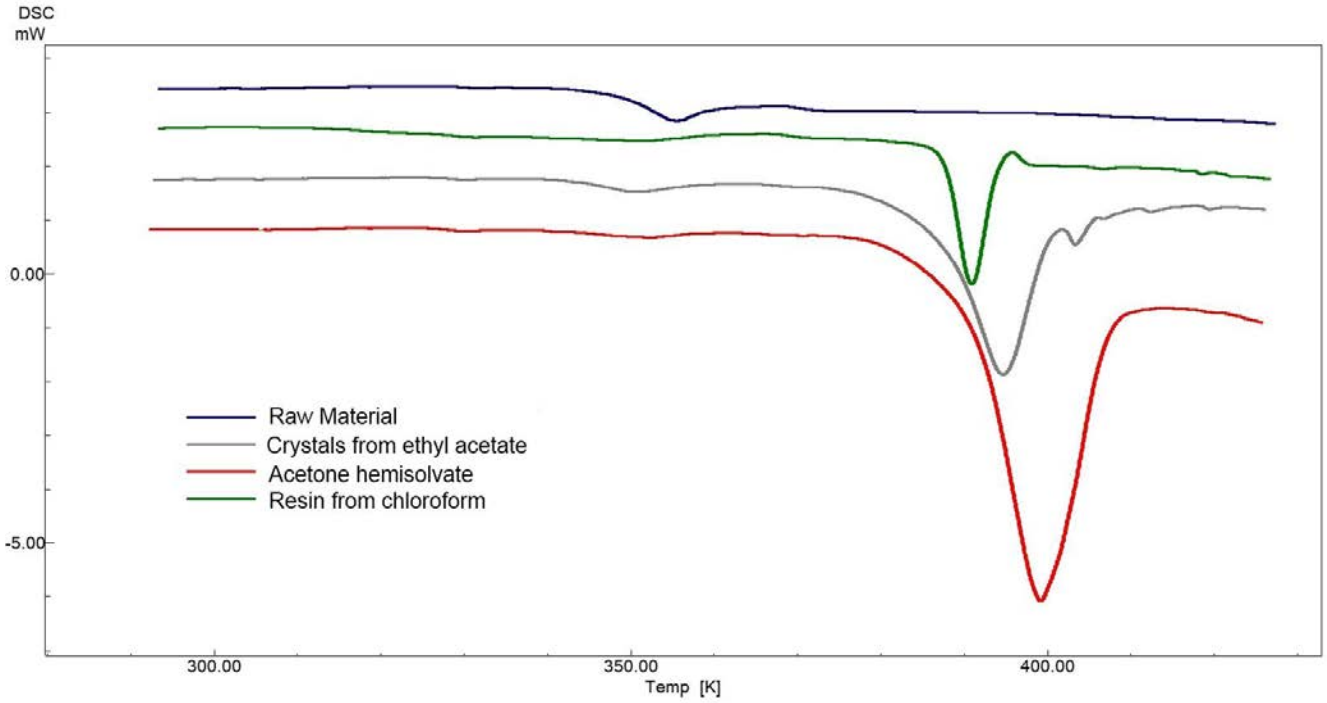

Figure S1: DSC curves of lopinavir raw material and its recrystallisation products.

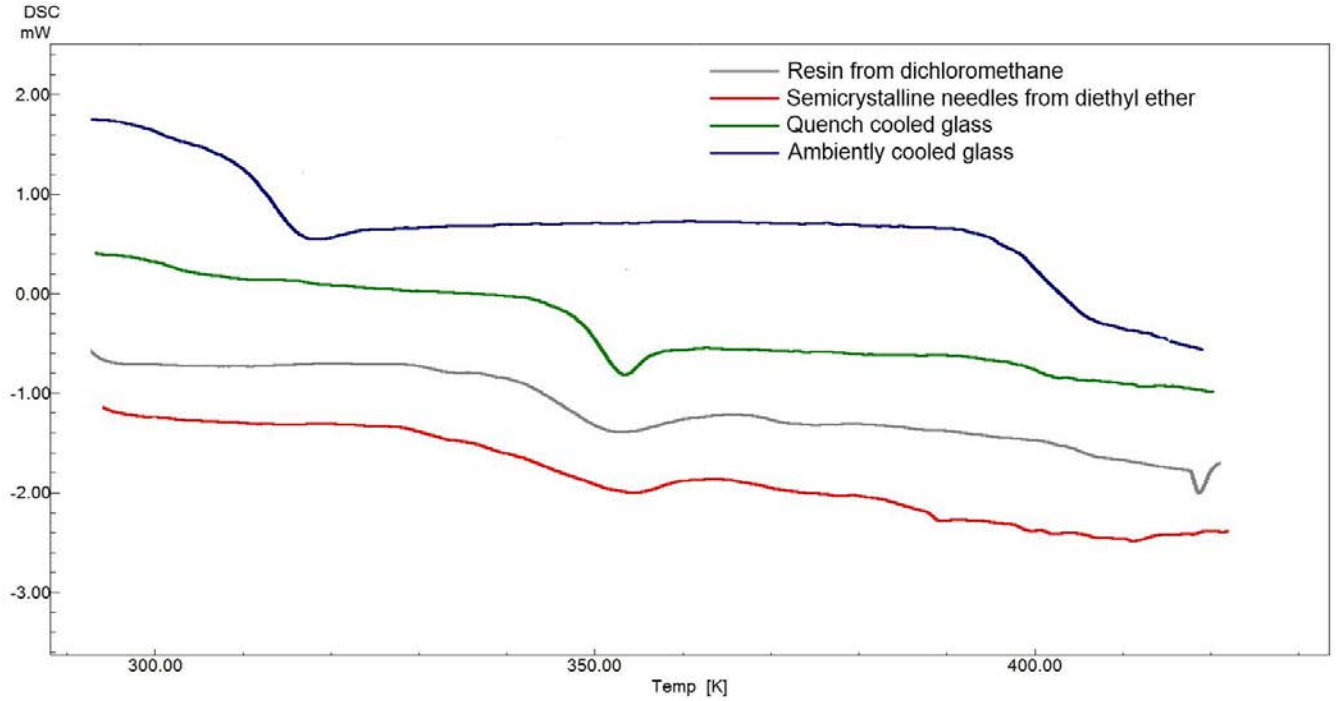

Figure S2: DSC curves of lopinavir glasses, resin from dichloromethane and needles from diethyl ether.

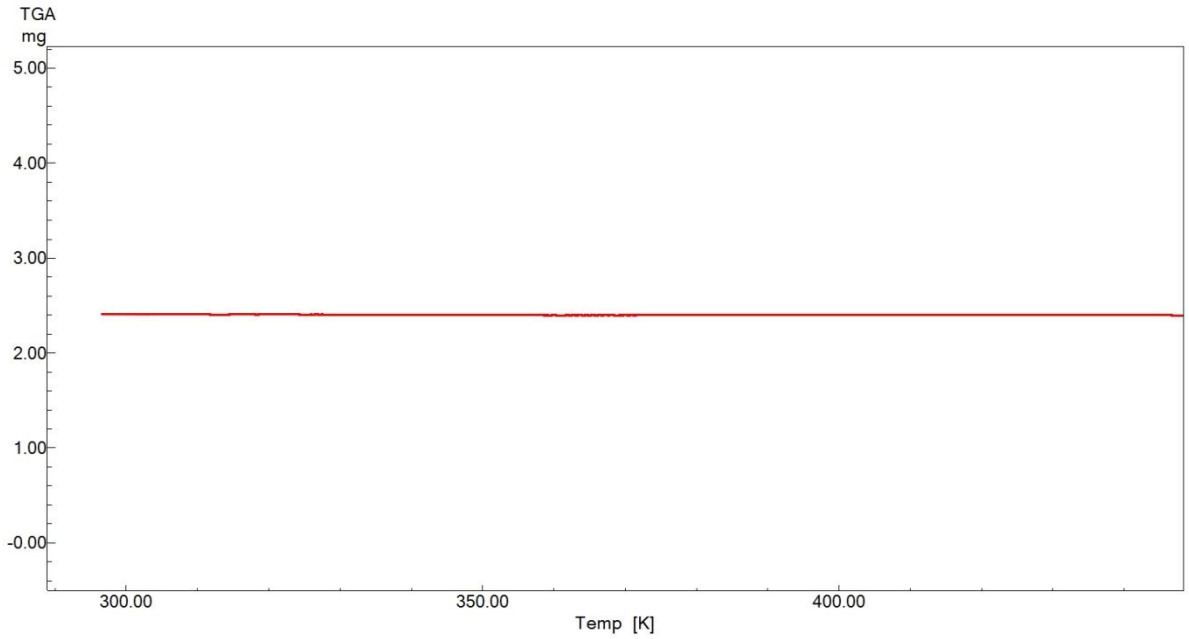

Figure S3: TGA of lopinavir raw material.

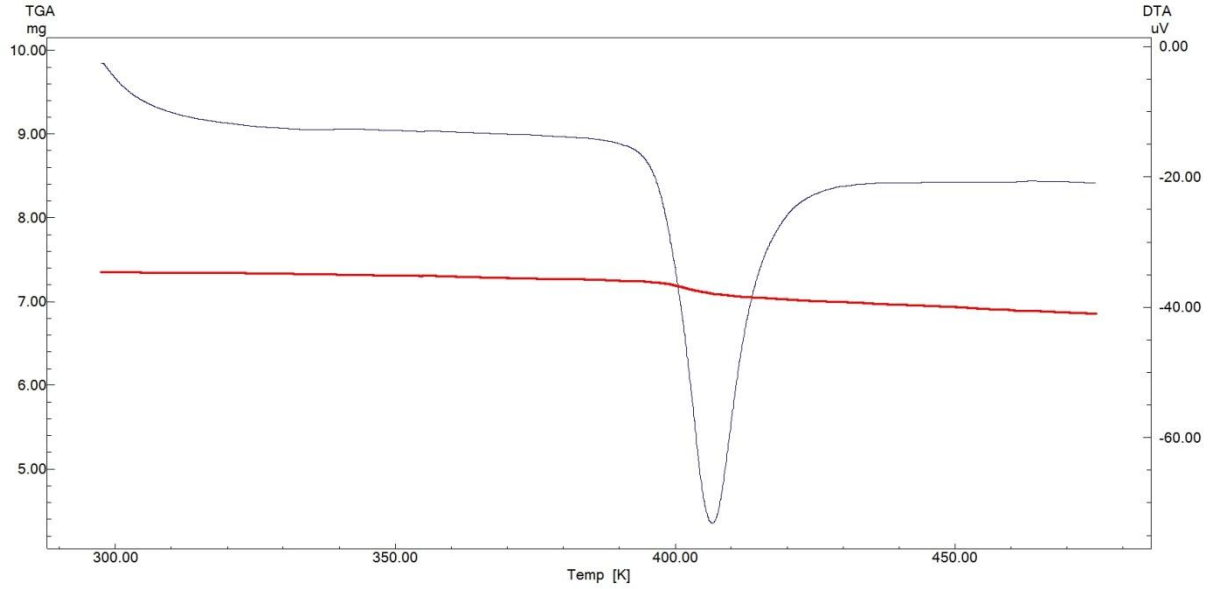

Figure S4: TGA of lopinavir crystals from ethyl acetate.

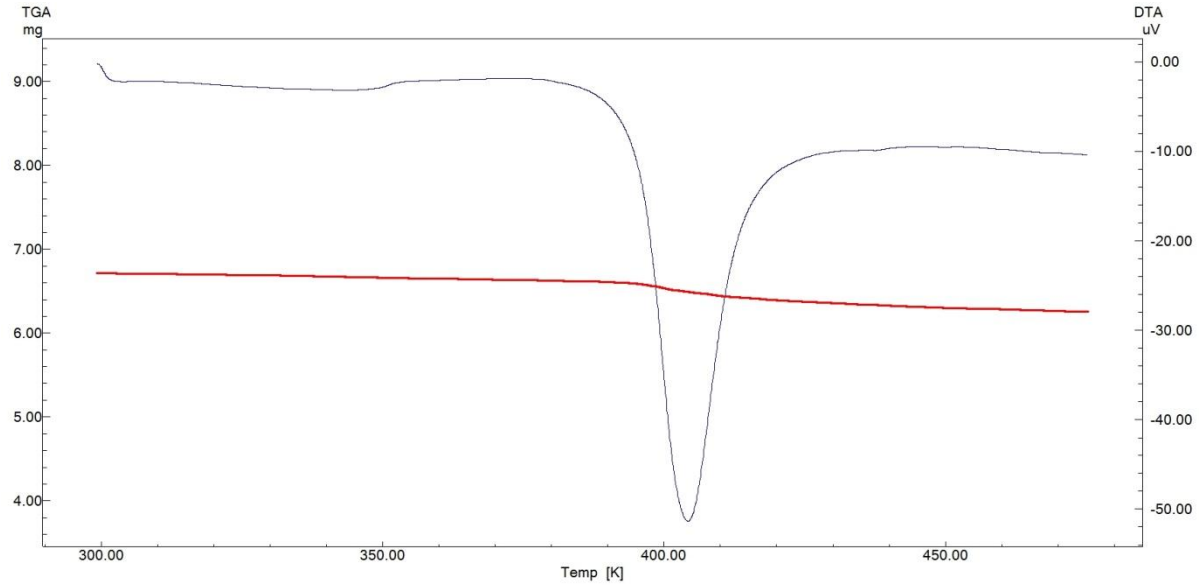

Figure S5: TGA of lopinavir crystals from acetone.

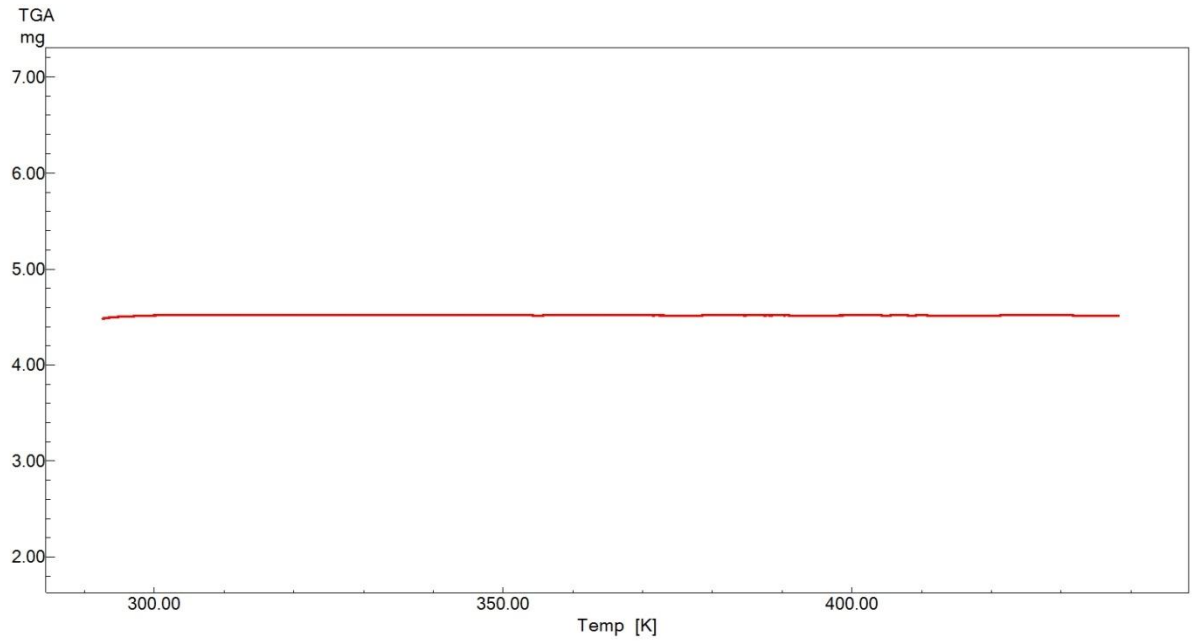

Figure S6: TGA of lopinavir needles from diethyl ether.

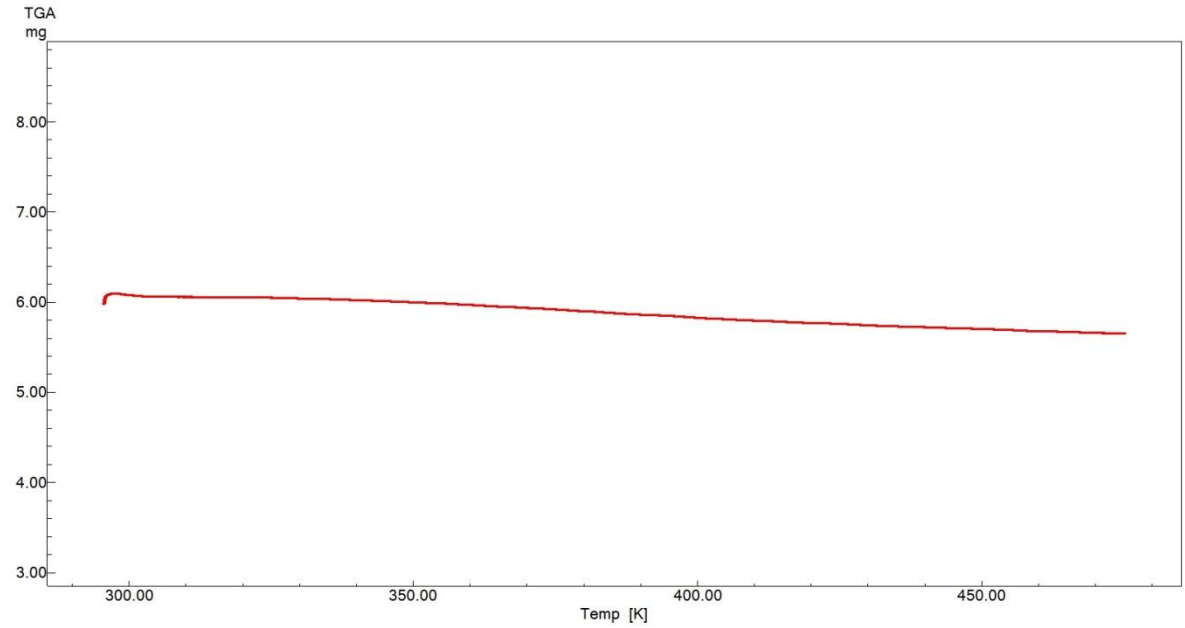

Figure S7: TGA of lopinavir resin from chloroform.

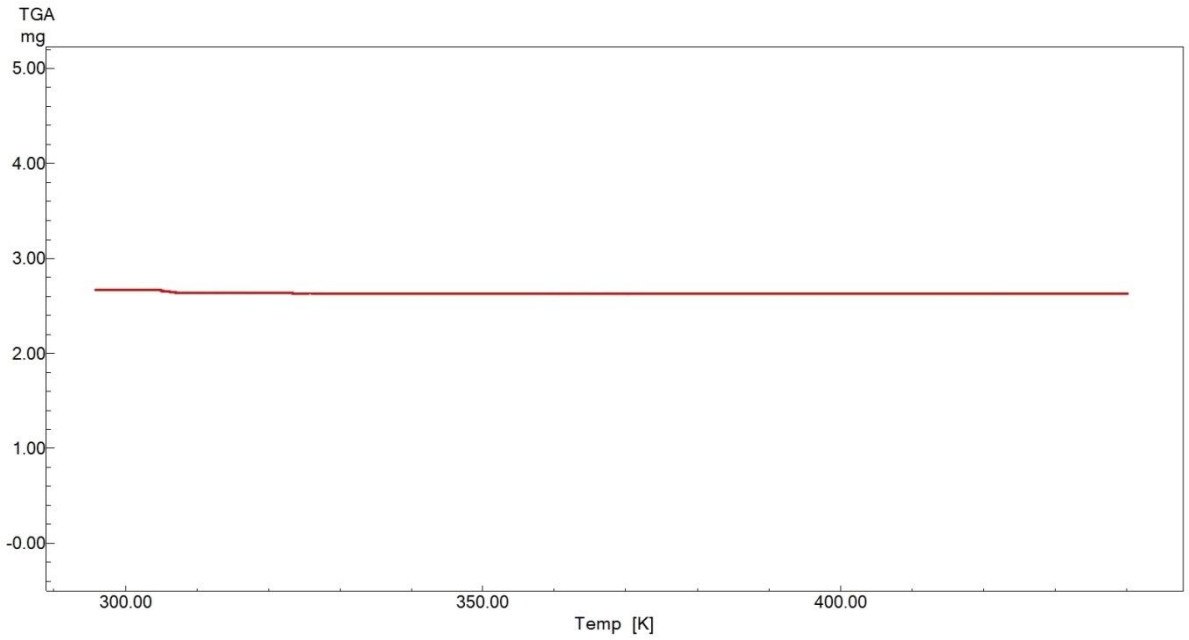

Figure S8: TGA of lopinavir resin from dischloromethane.

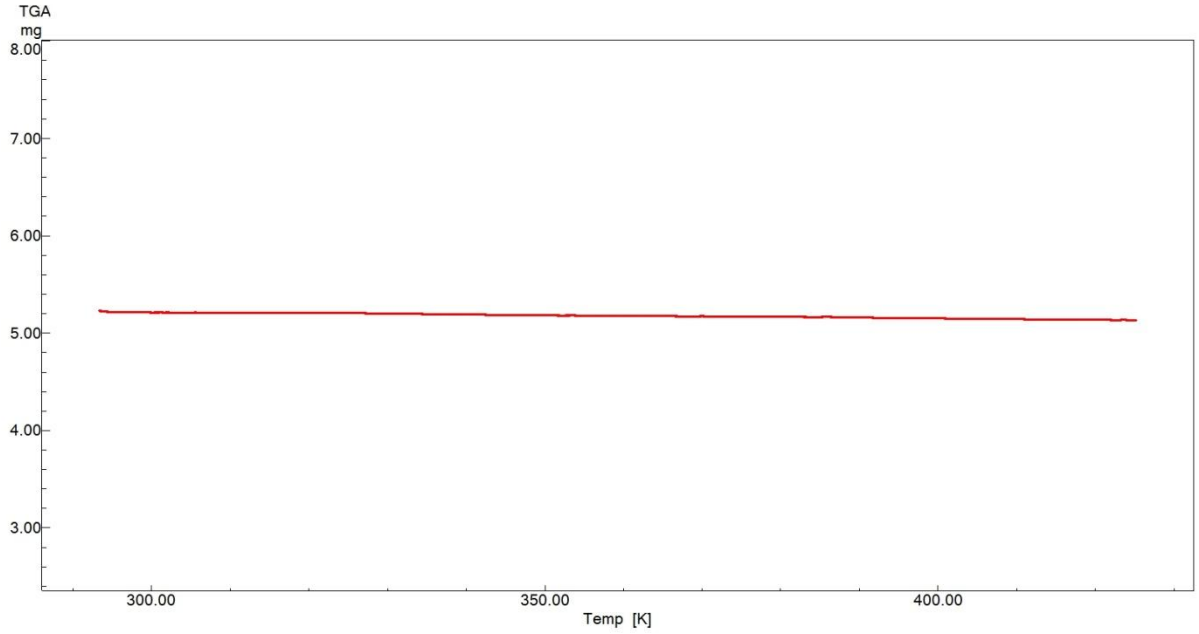

Figure S9: TGA of lopinavir glass cooled at ambient temperature.

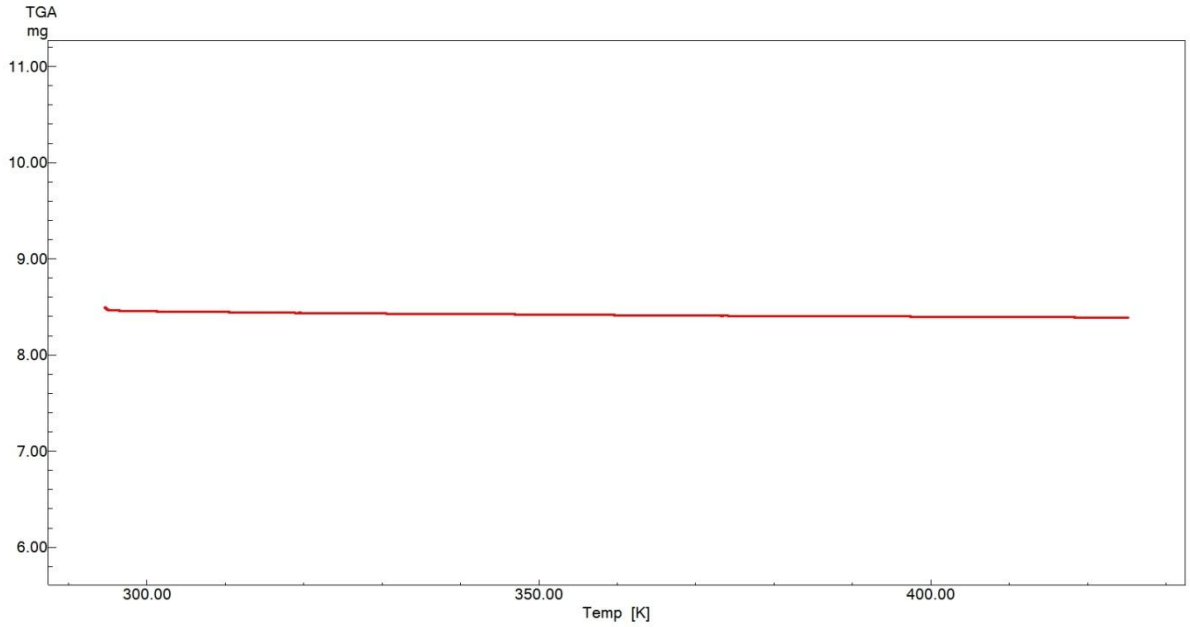

Figure S10: TGA of quench cooled lopinavir glass.

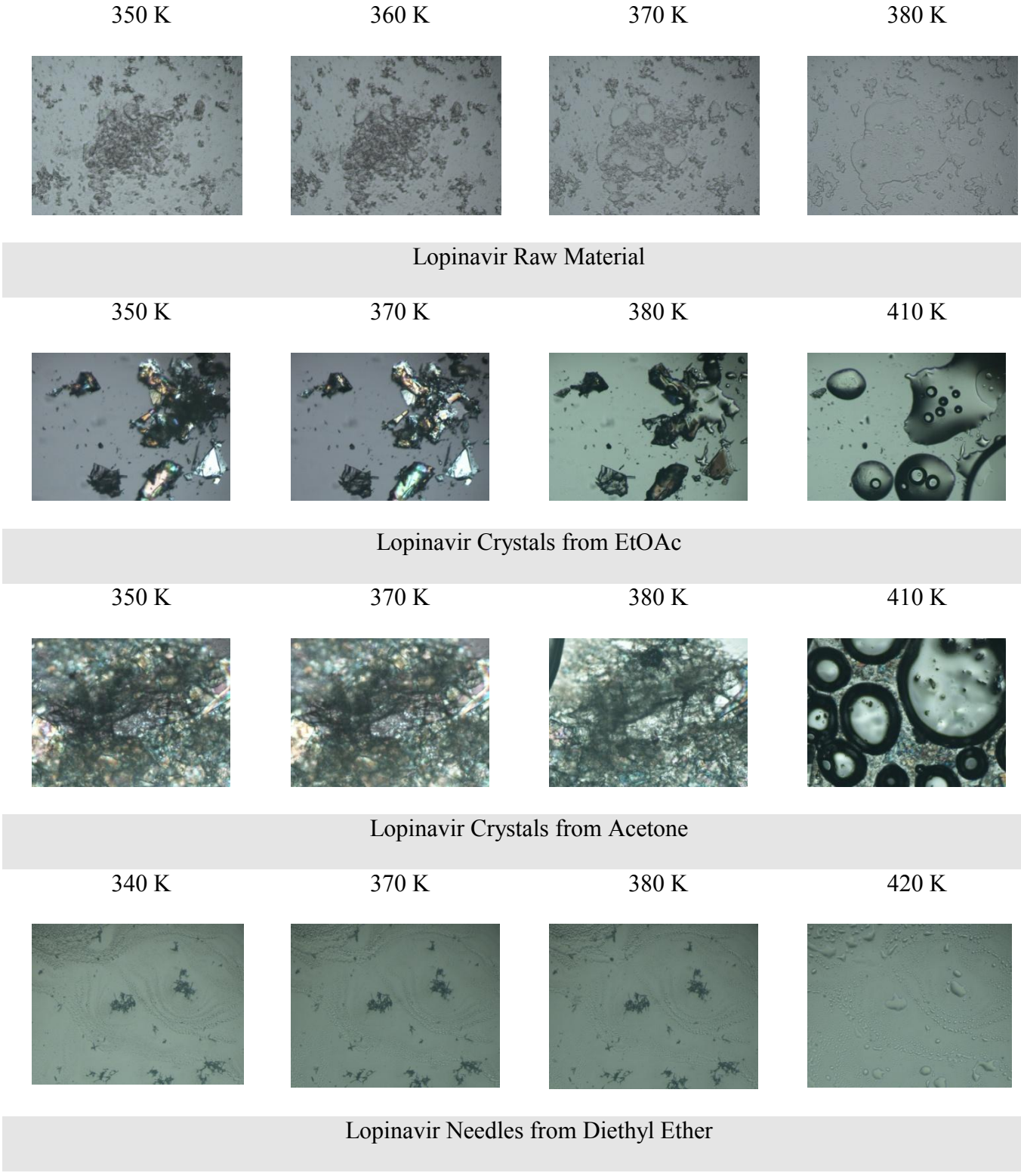

Figure S11: Hot stage micrographs of lopinavir raw material and crystals.

340 K | 370 K | 380 K | 410 K

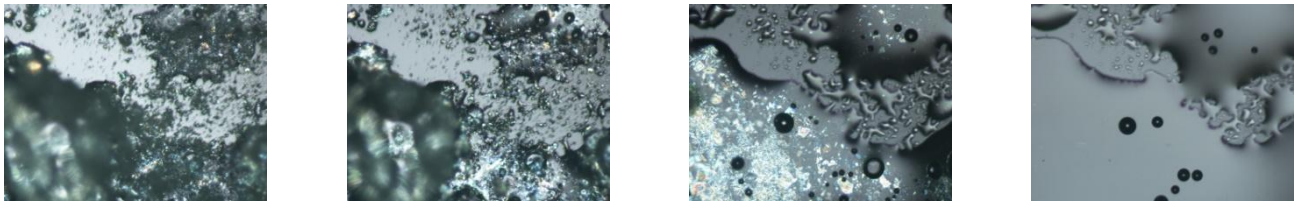

Lopinavir Resin from $CHCl_3$

340 K | 360 K | 380 K | 420 K

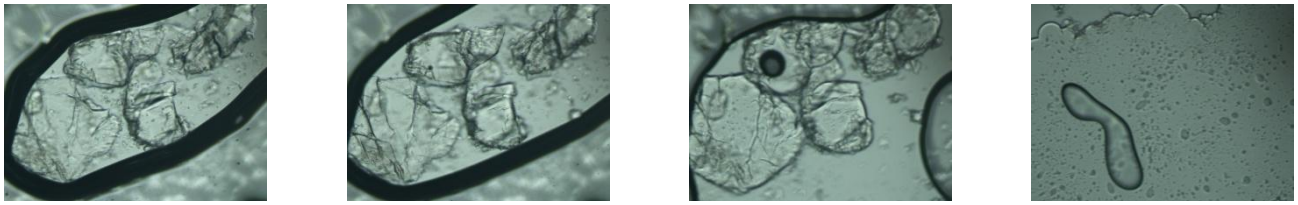

Lopinavir Resin from Dichloromethane

300 K | 320 K | 340 K | 410 K

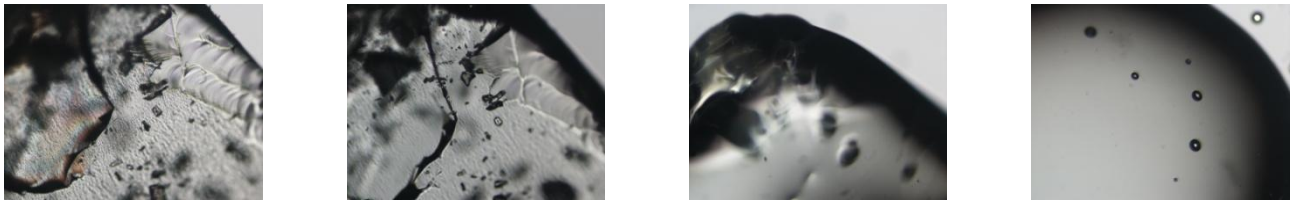

Slowly Cooled Lopinavir Glass

340 K | 380 K | 400 K | 450 K

Quench Cooled Lopinavir Glass

Figure S12: Hot stage micrographs of lopinavir resins and glasses.

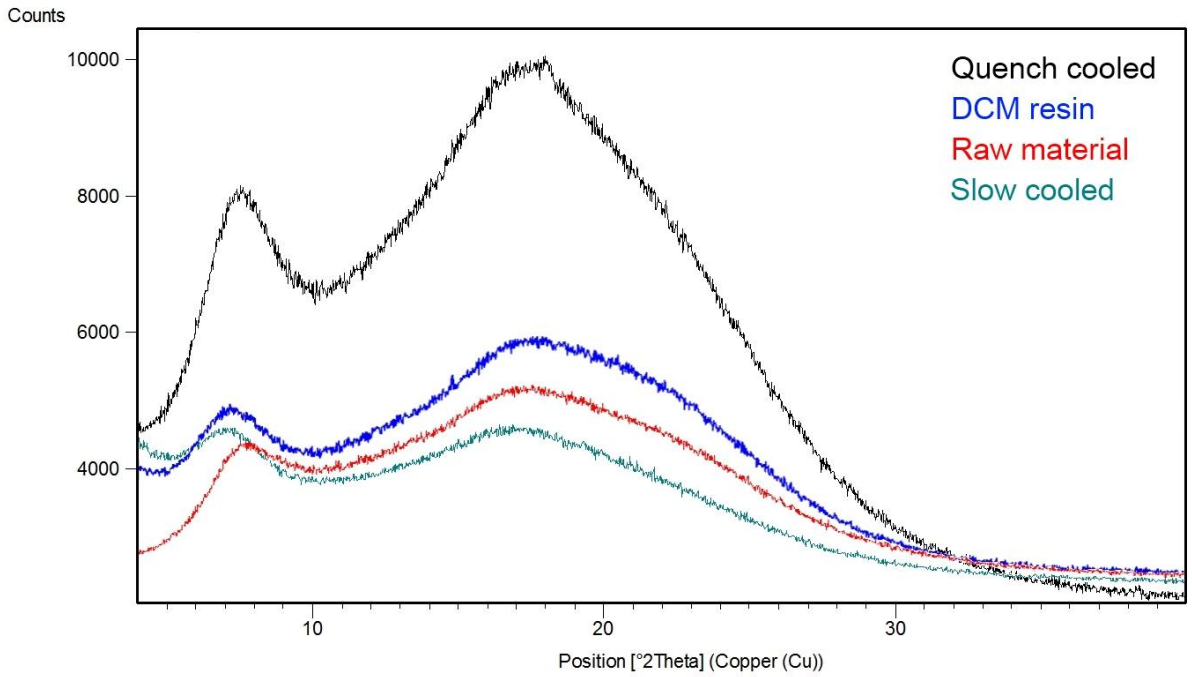

Figure S13: PXRD analysis of lopinavir raw material and its amorphous products.

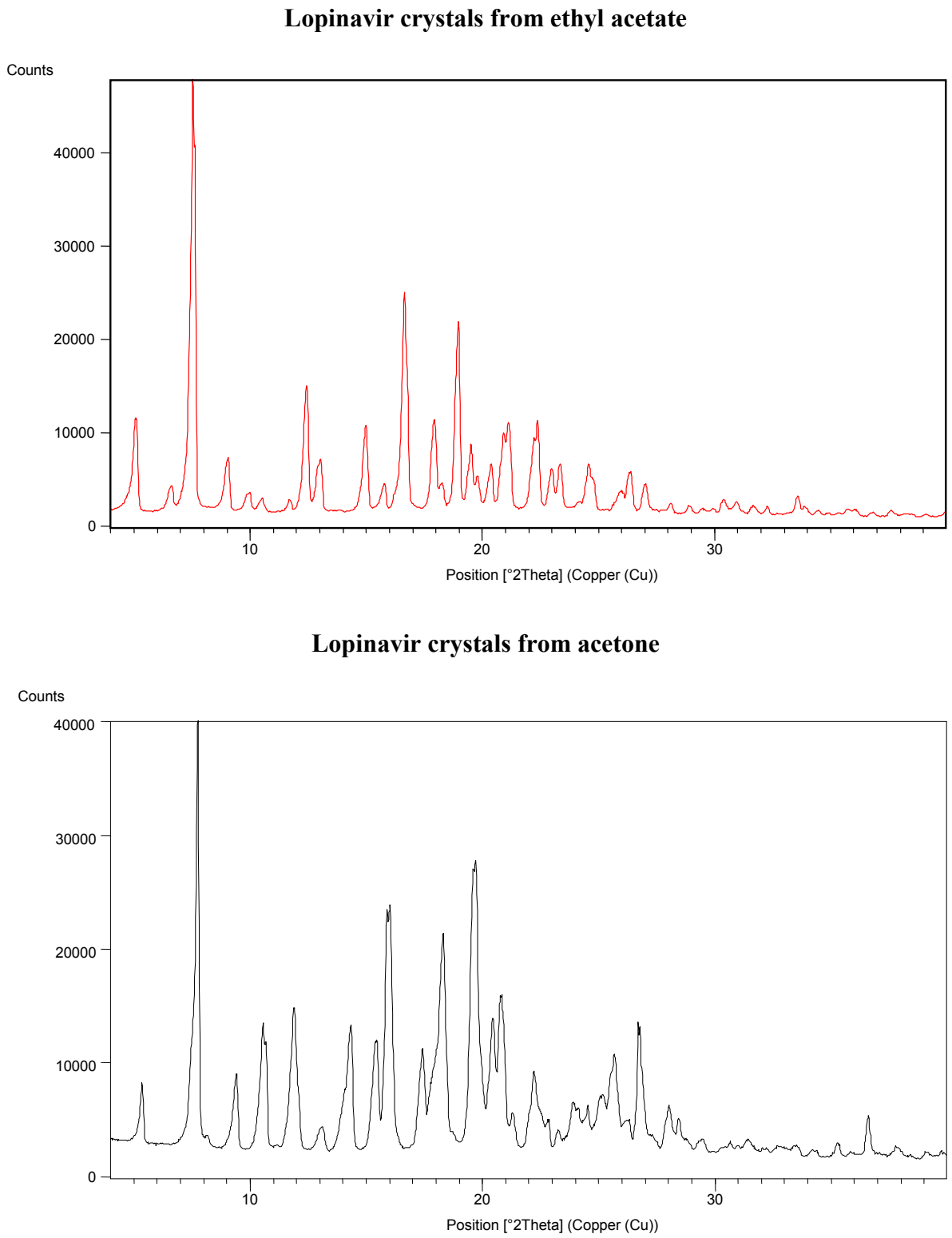

Figure S14: PXRD diffractograms of lopinavir crystals obtained from ethyl acetate and acetone.

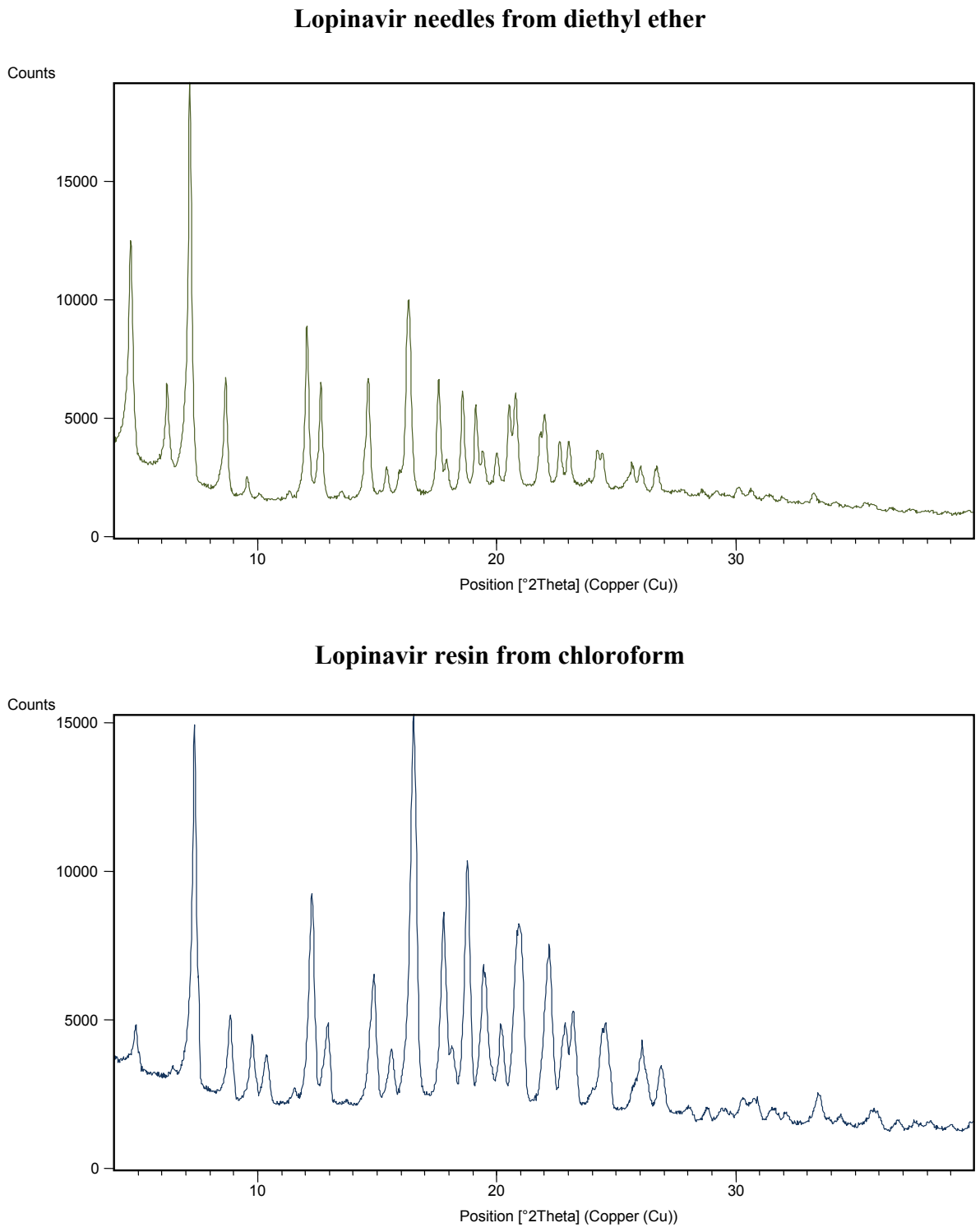

Figure S15: PXRD diffractograms of lopinavir needles from diethyl ether and lopinavir resin from chloroform.

Lopinavir Raw Material

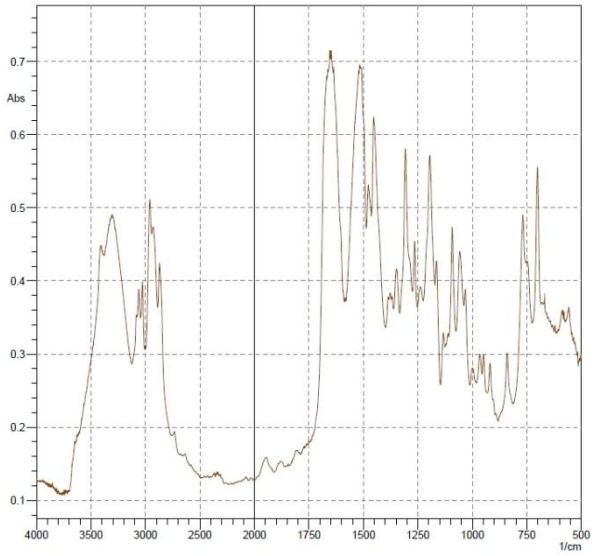

Lopinavir crystals from EtOAc

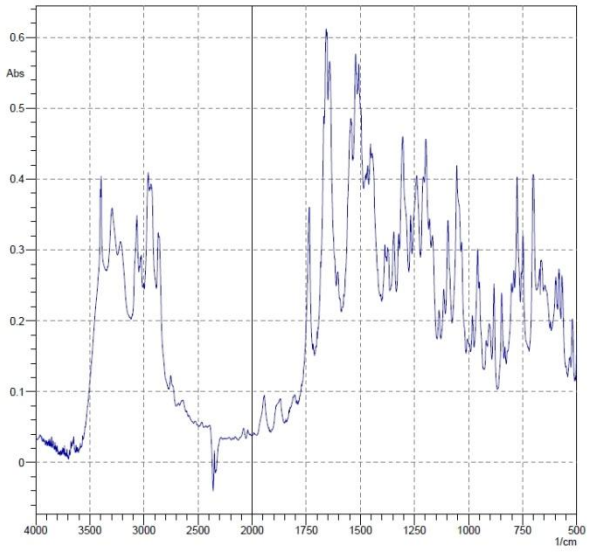

Lopinavir crystals from acetone

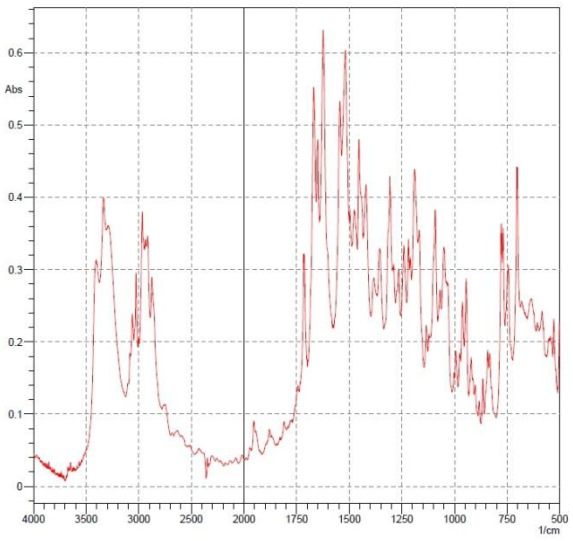

Lopinavir needles from diethyl ether

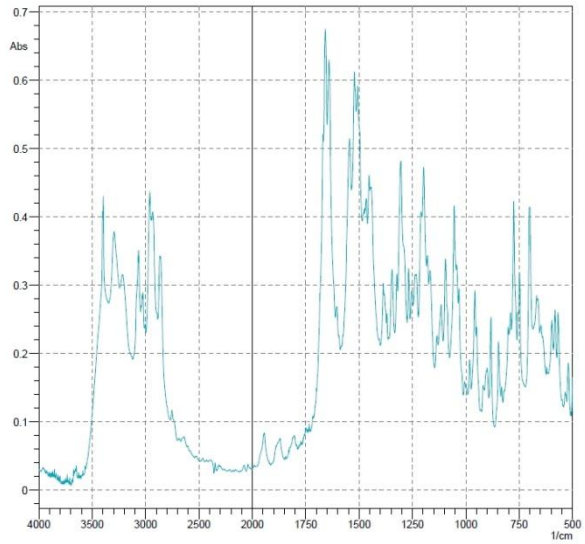

Figure S16: FTIR interferograms of lopinavir raw material and its recrystallisation products.

Lopinavir resin from chloroform

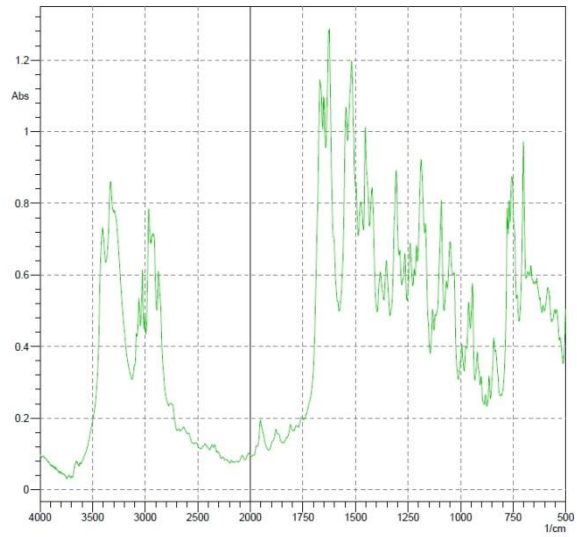

Lopinavir resin from DCM

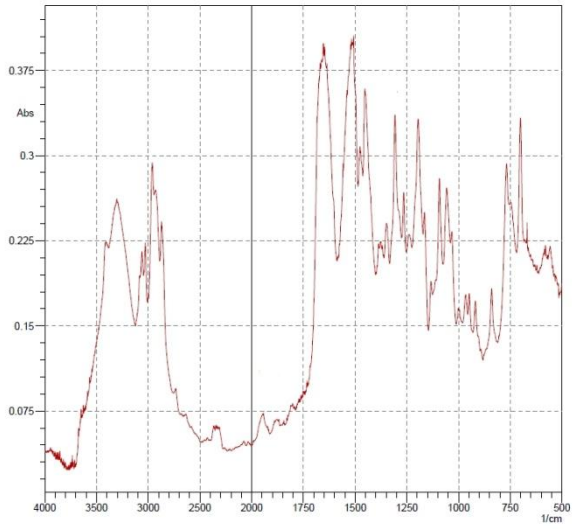

Slowly cooled glass

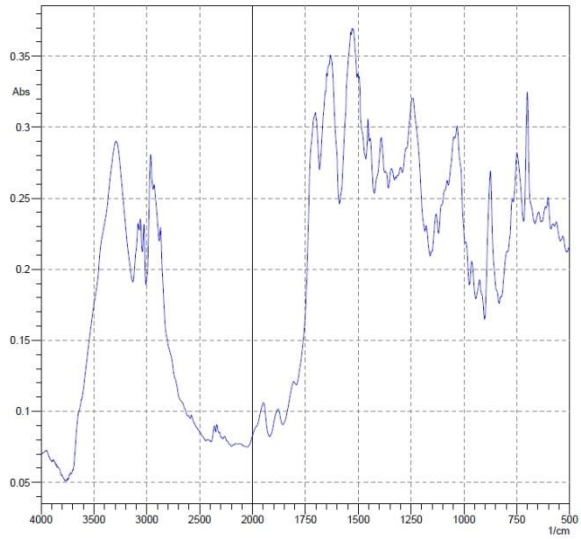

Quench cooled glass

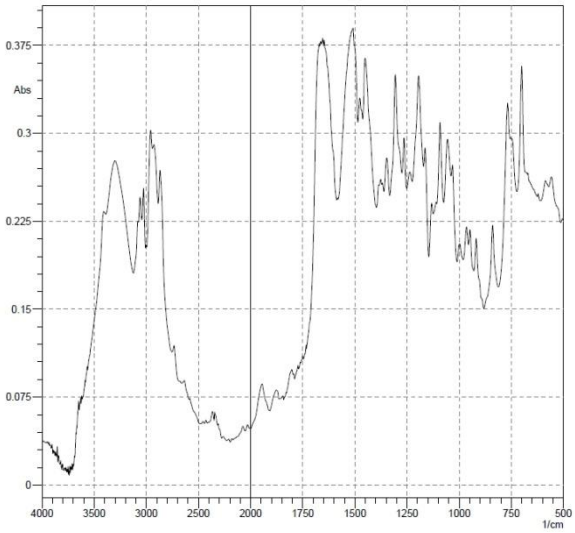

Figure S17: FTIR interferograms of lopinavir resins and glasses.

Lopinavir raw material

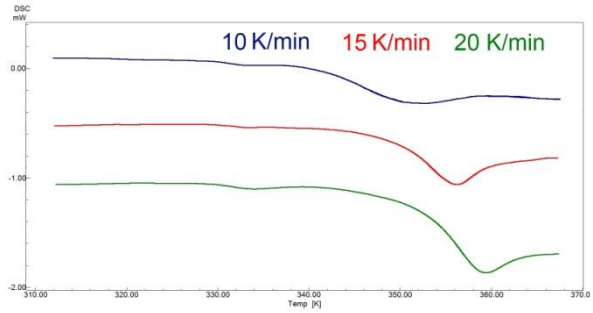

Lopinavir crystals from EtOAc

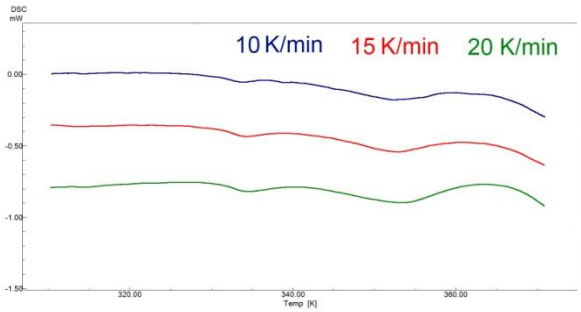

Lopinavir crystals from acetone

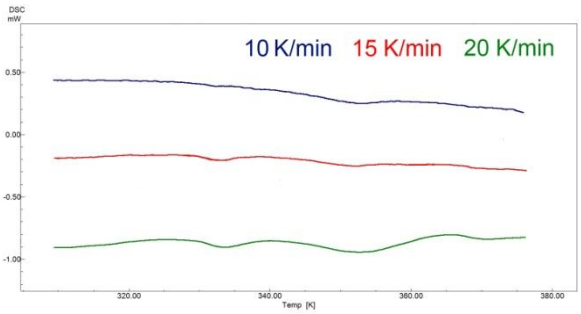

Lopinavir needles from diethyl ether

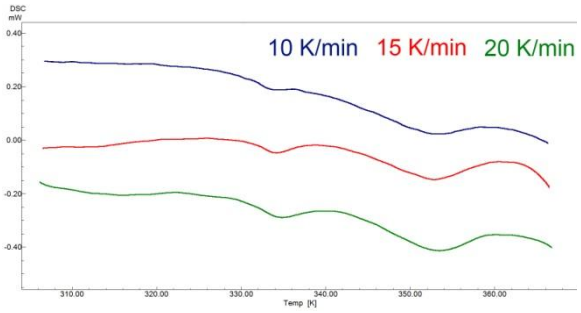

Lopinavir resin from $CHCl_3$

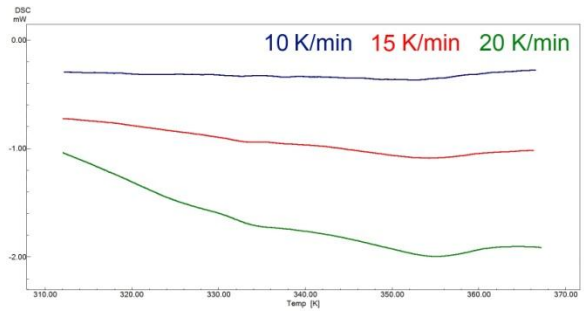

Lopinavir resin from DCM

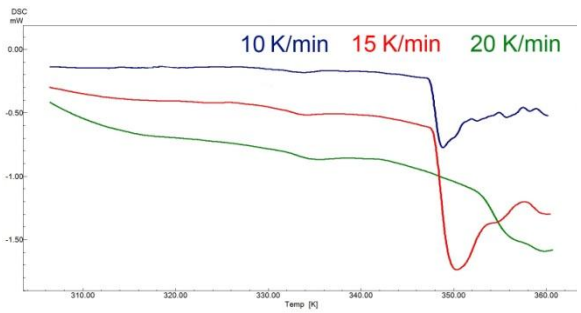

Slowly cooled lopinavir glass

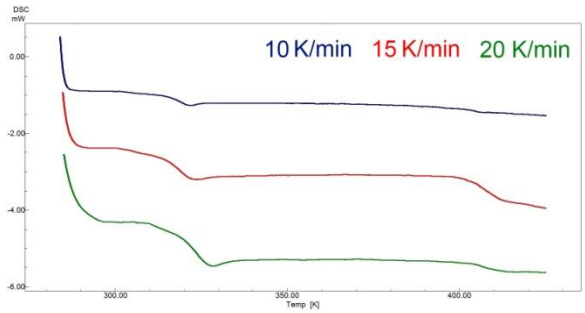

Quench cooled lopinavir glass

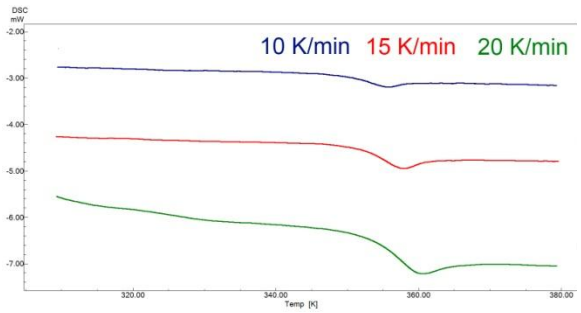

Figure S18: DSC curves showing the small β-relaxation endotherms followed by the larger α-relaxations.

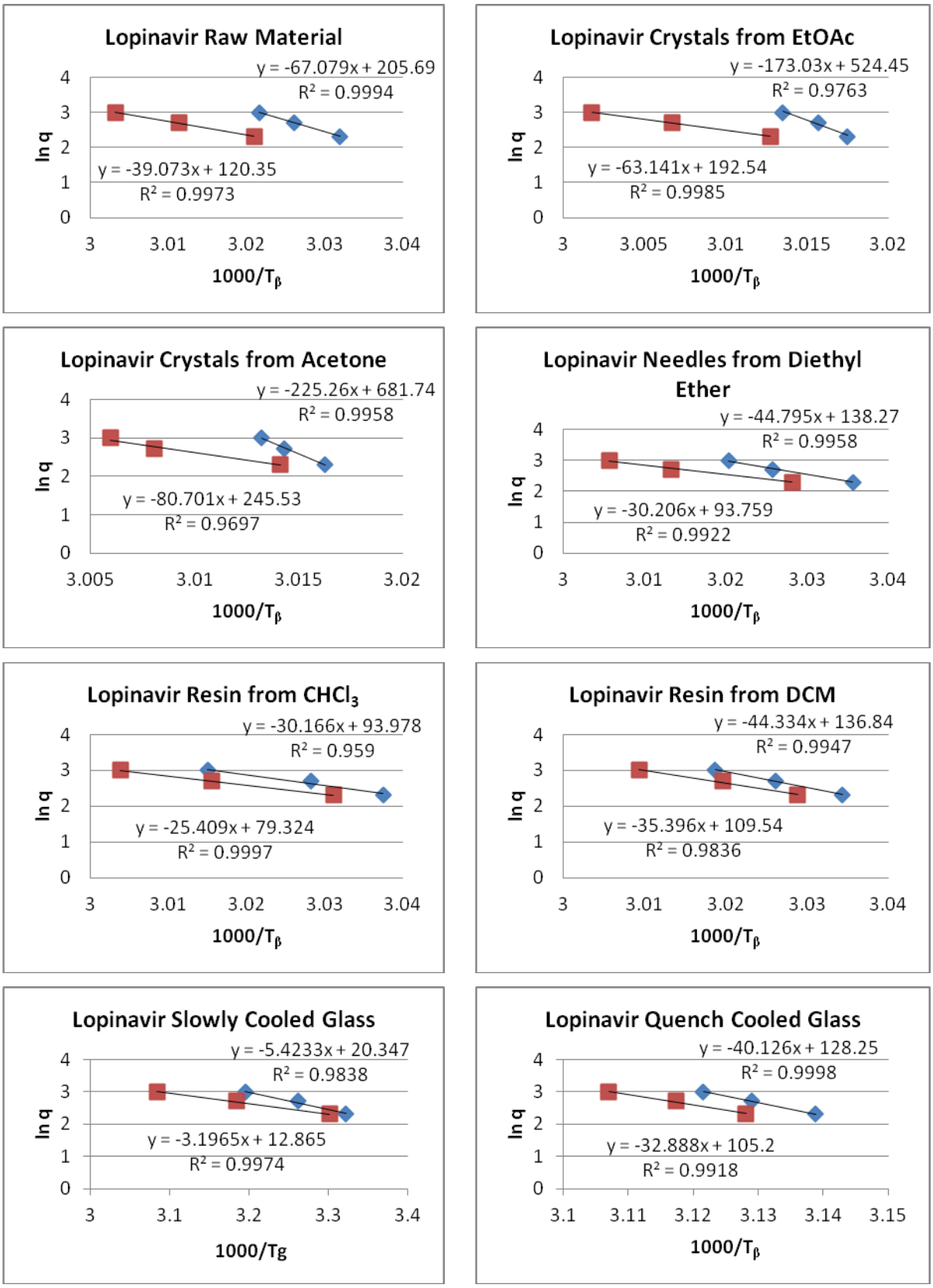

Figure S19: Arrhenius plots of T_β (blue diamonds) and T_β^{mid} (red squares) for each sample.

Lopinavir raw material

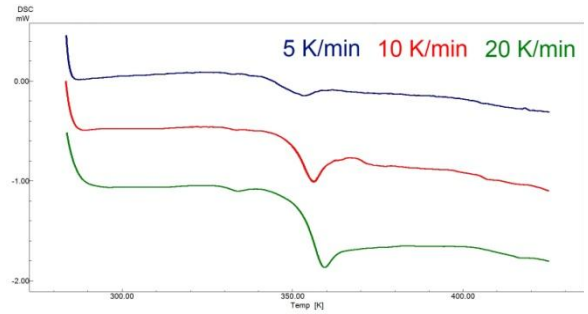

Lopinavir crystals from EtOAc

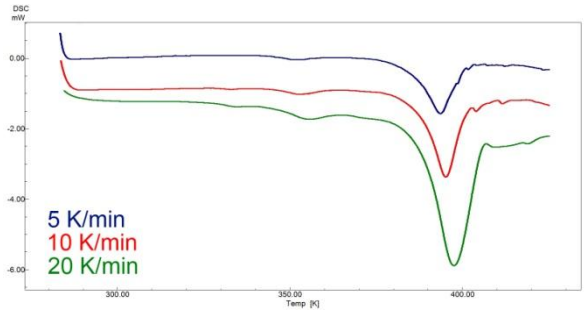

Lopinavir crystals from acetone

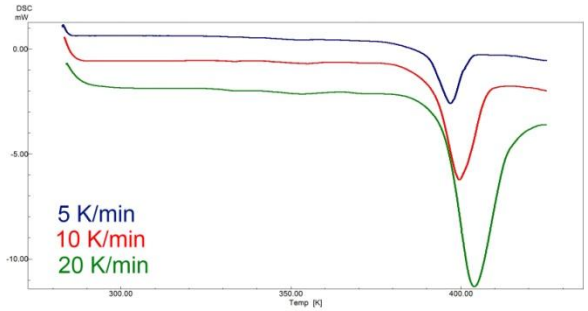

Lopinavir needles from diethyl ether

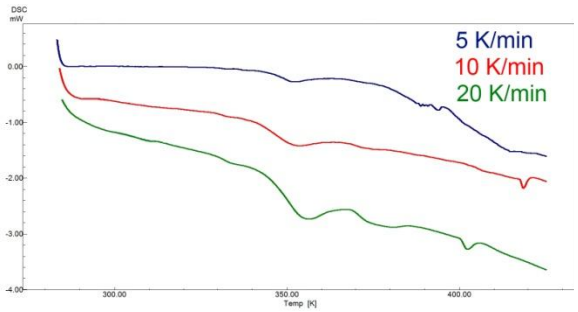

Lopinavir resin from $CHCl_3$

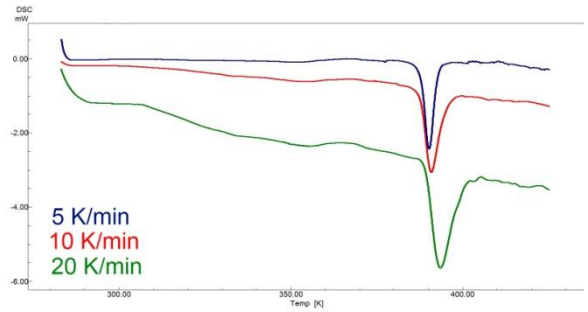

Lopinavir resin from DCM

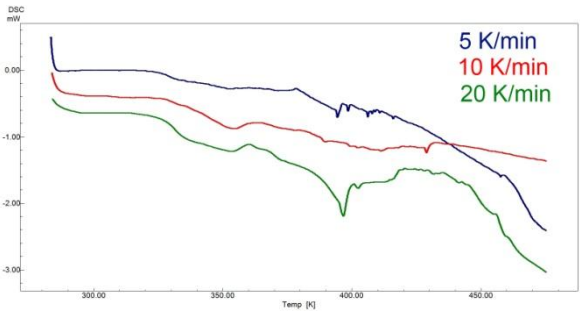

Slowly cooled lopinavir glass

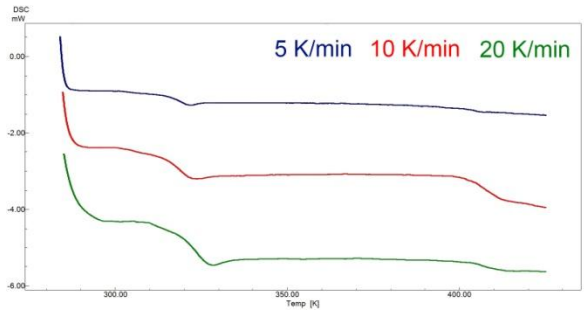

Quench cooled lopinavir glass

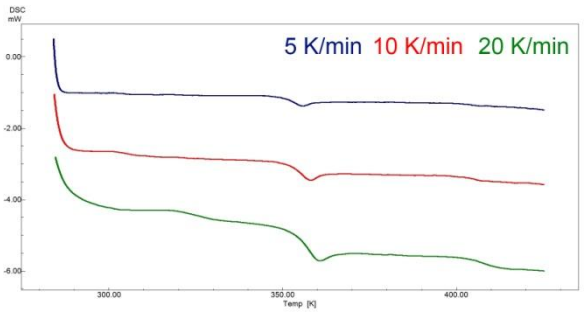

Figure S20: DSC curves showing the shifts in T_g with heating rate.

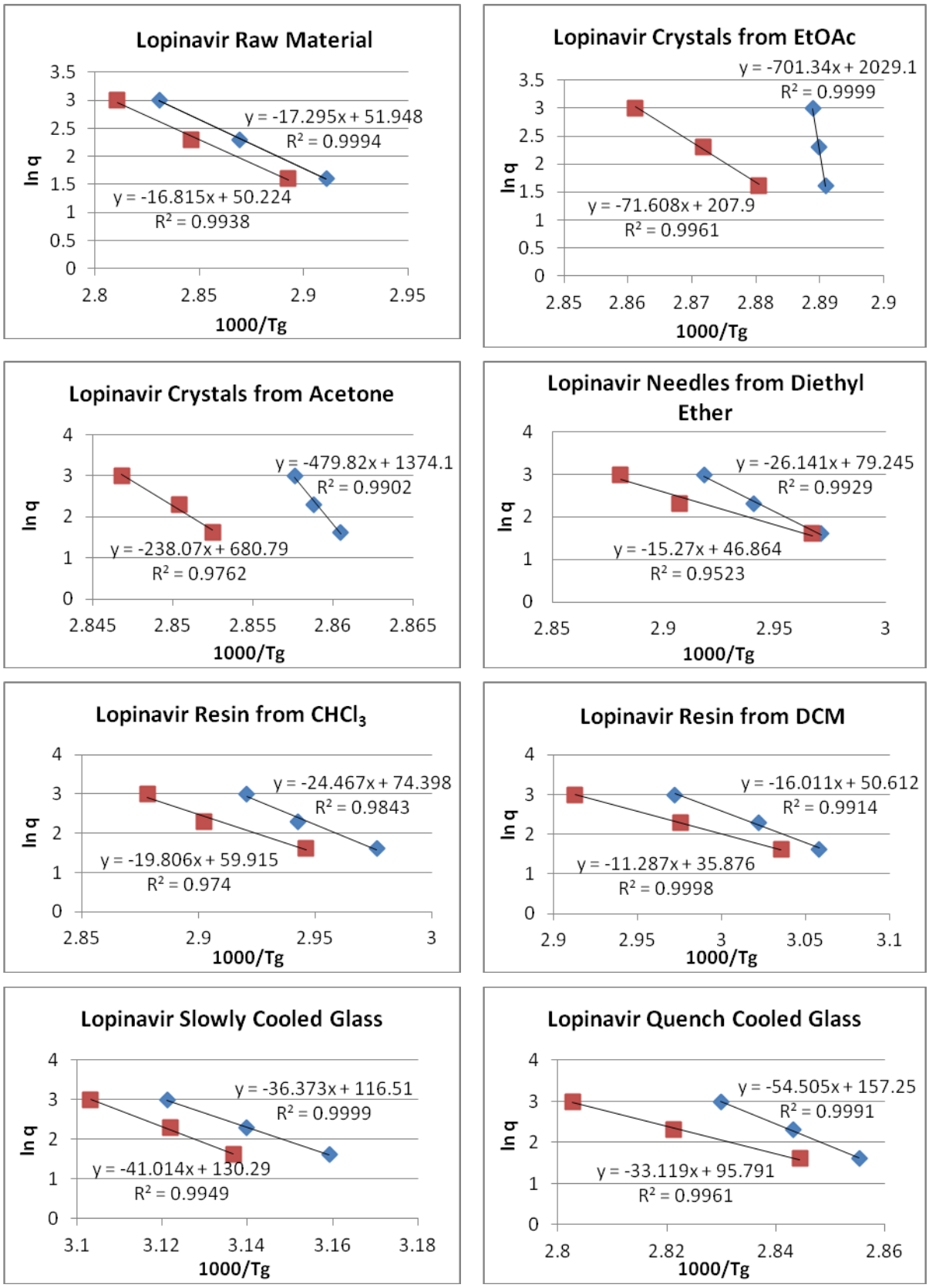

Figure S21: Arrhenius plots of T_g (blue diamonds) and T_g^{mid} (red squares) for each sample.

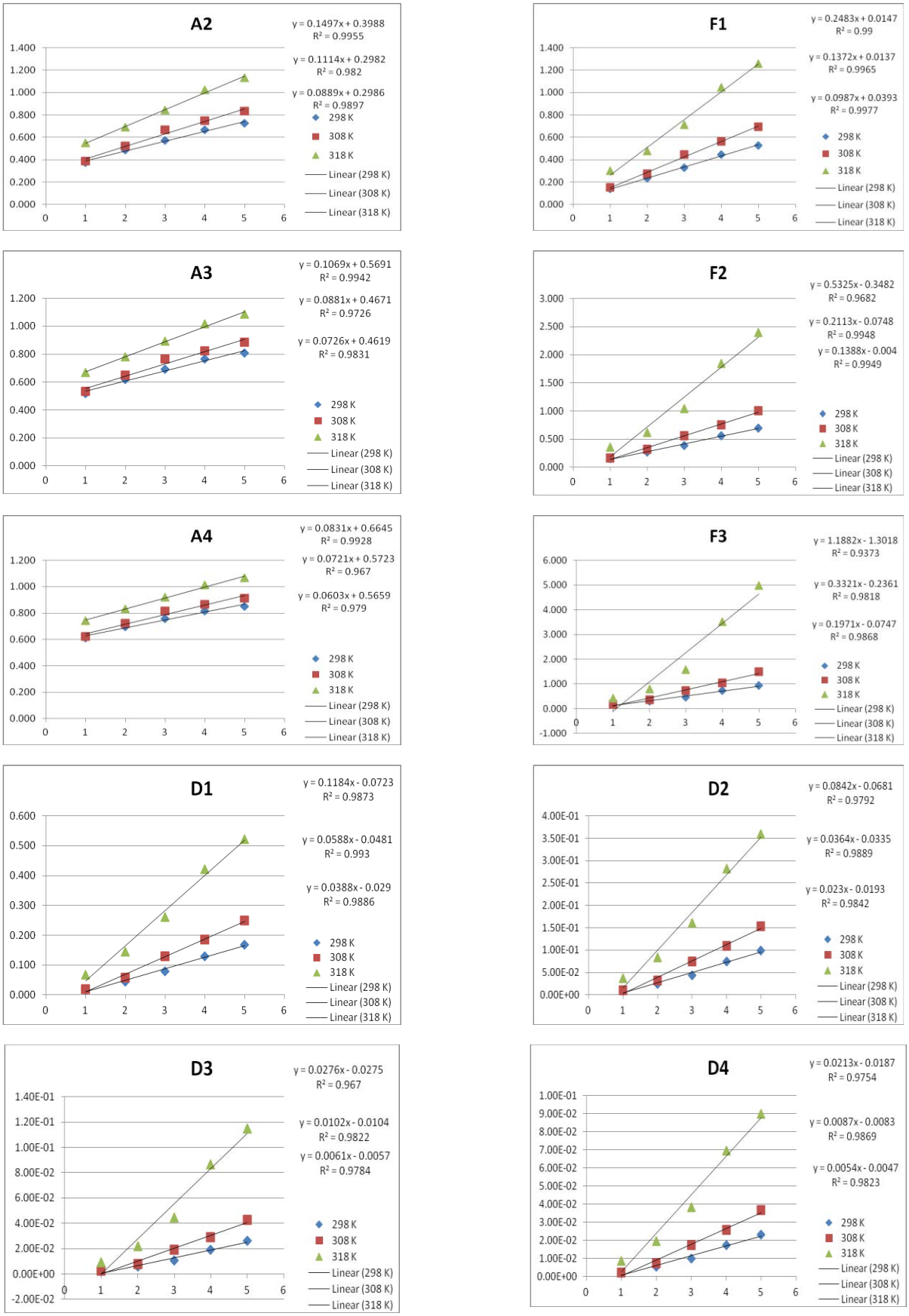

Figure S22: Model fitting results for lopinavir crystals from ethyl acetate.

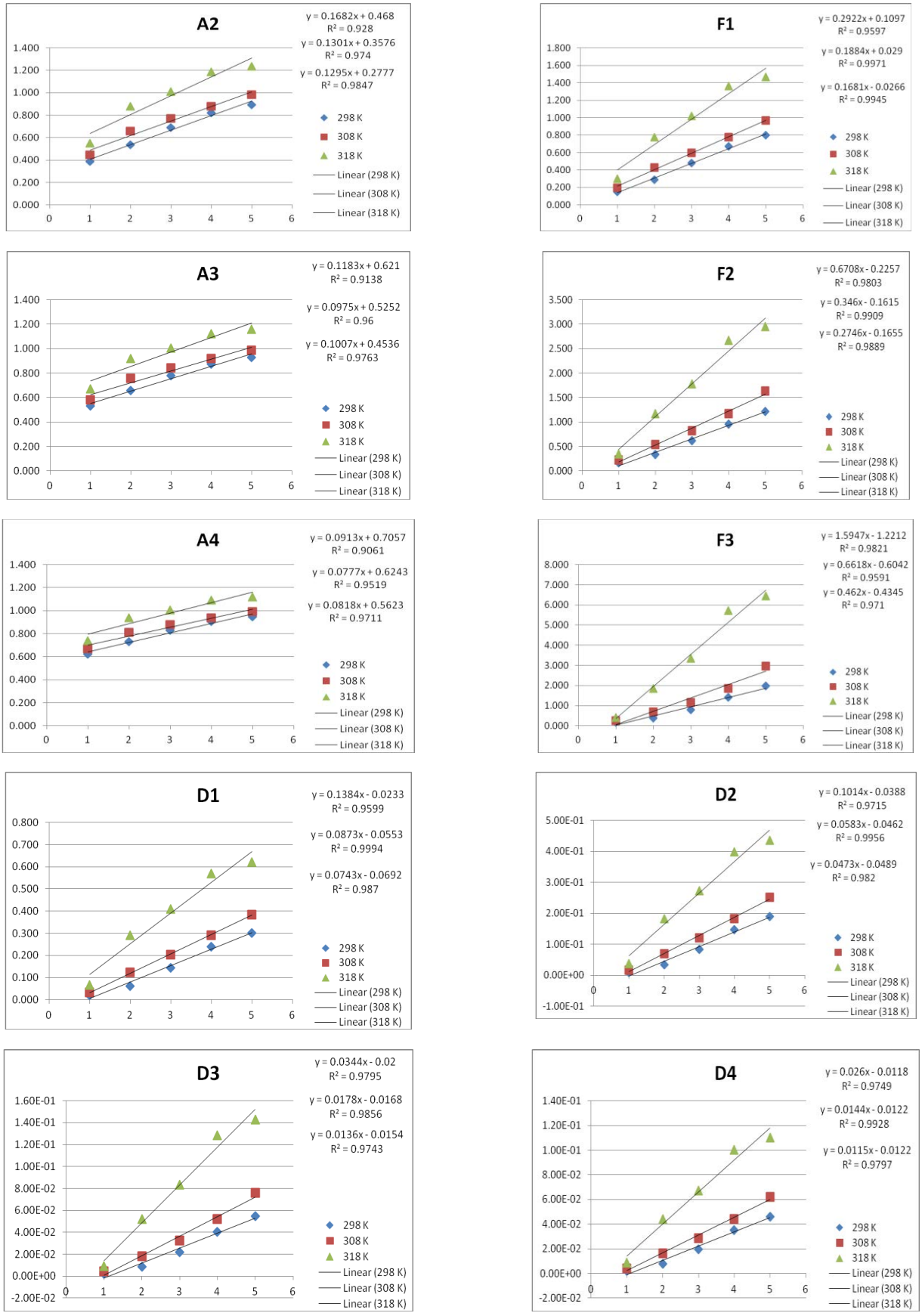

Figure S23: Model fitting results for quench cooled lopinavir glass.

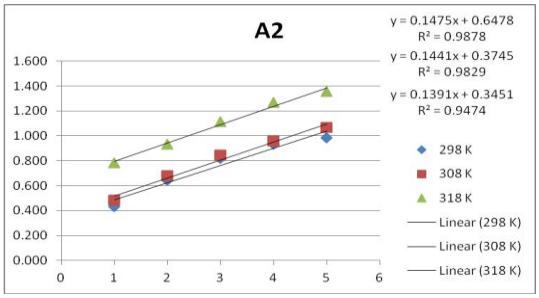

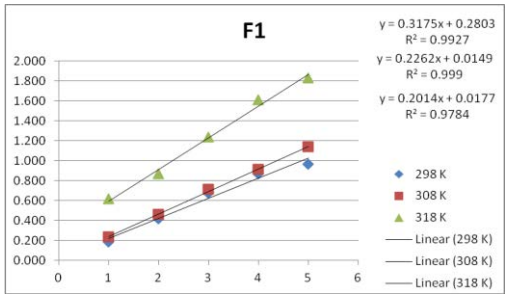

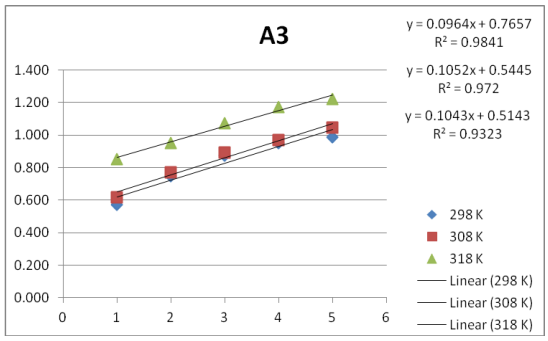

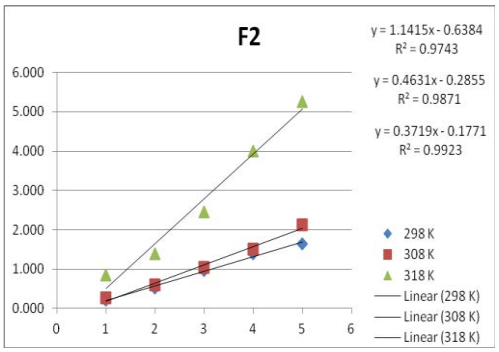

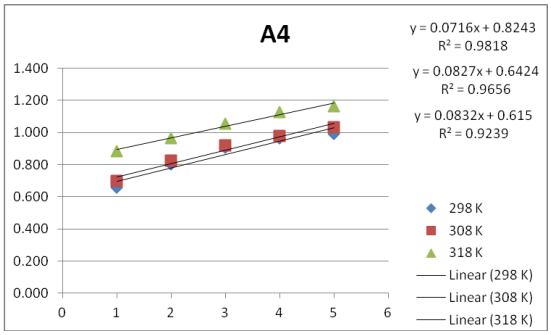

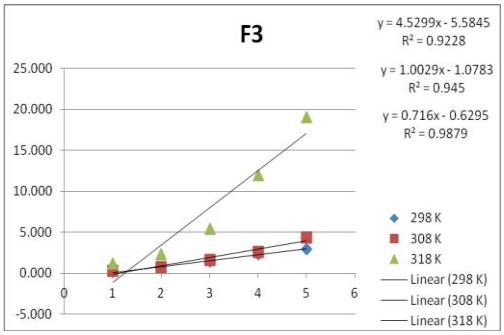

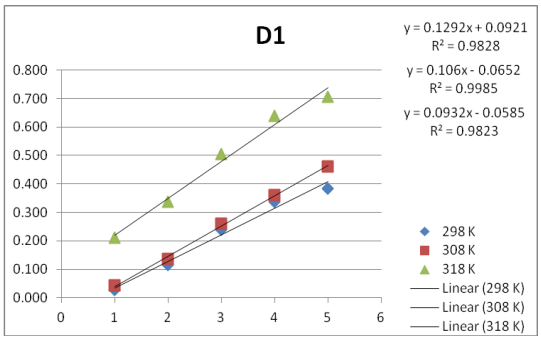

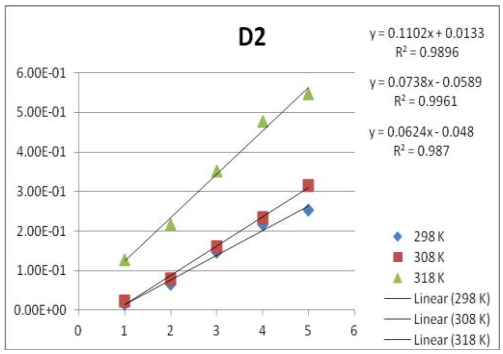

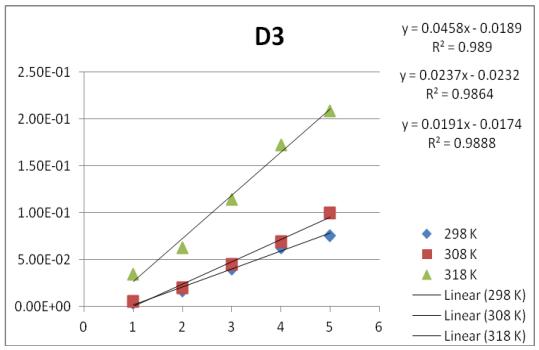

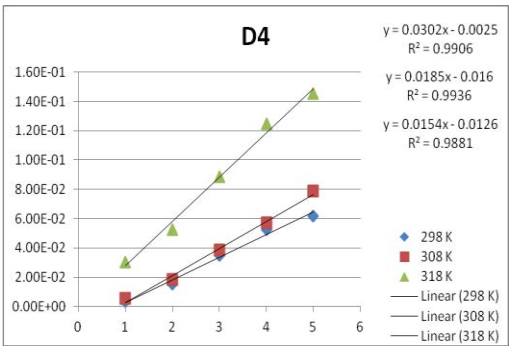

Figure S24: Model fitting results for lopinavir glass cooled at ambient temperature.

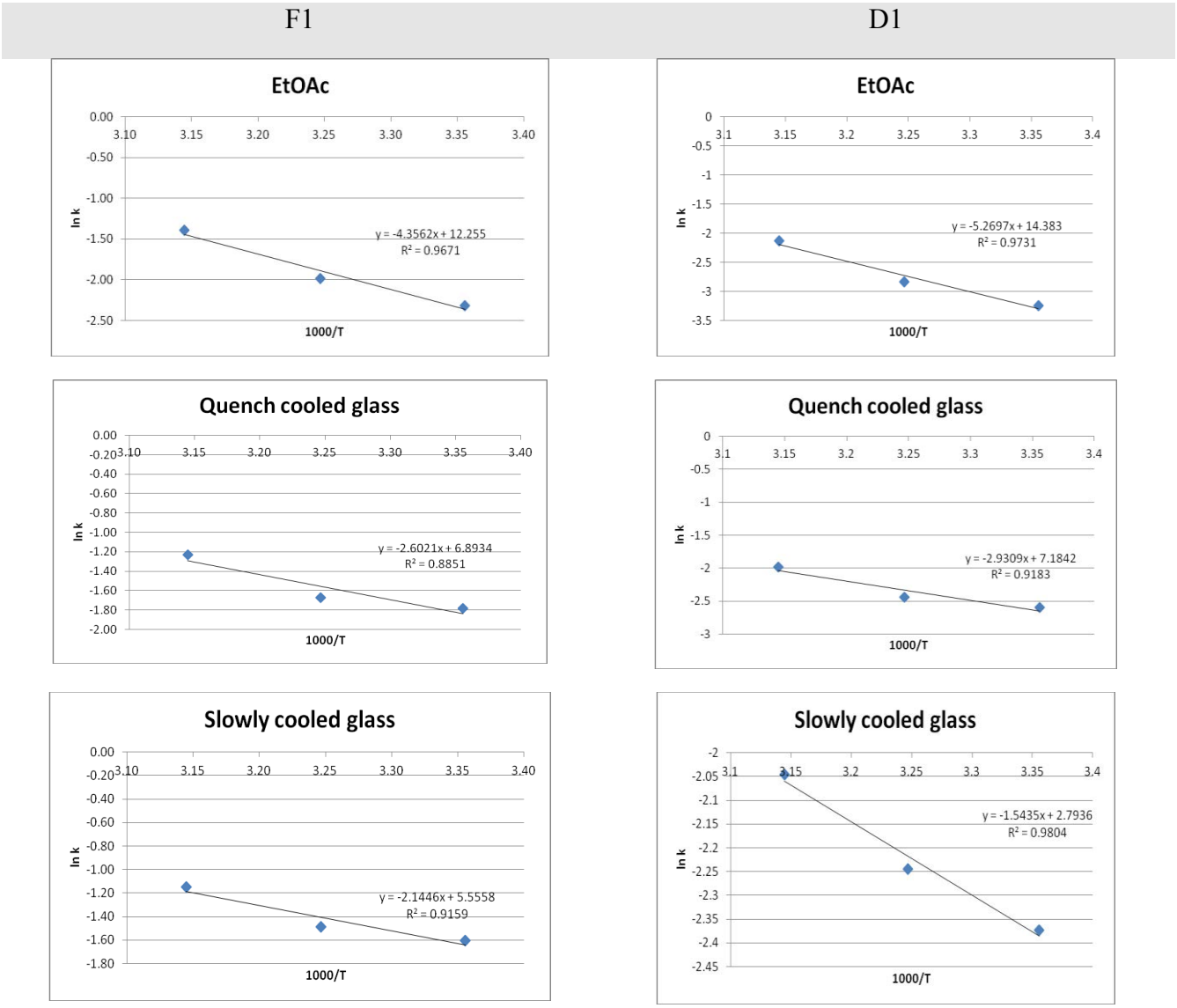

Figure S25: Arrhenius plots of the natural logarithms of the slopes determined from the model fitting for first-order kinetics and one-dimensional diffusion (since D1 exhibited the second best fit).

Table S1: T_β and T_β^{mid} of lopinavir raw material, its recrystallisation products and glasses (mean ± S.D.)

Preparation conditions	T_β (K)			T_β^{mid} (K)		
	10 K/min	15 K/min	20 K/min	10 K/min	15 K/min	20 K/min
Raw material	330 ± 1.6	330 ± 1.1	331 ± 0.0	331 ± 1.7	332 ± 0.8	333 ± 0.1
Ethyl acetate	331 ± 0.2	331 ± 0.5	332 ± 0.1	332 ± 0.2	333 ± 0.4	333 ± 0.2
Acetone	331 ± 1.2	332 ± 0.0	332 ± 0.1	332 ± 0.9	332 ± 0.4	333 ± 0.0
Diethyl ether	329 ± 0.2	330 ± 0.3	331 ± 0.2	330 ± 0.1	332 ± 0.3	333 ± 0.1
Chloroform	329 ± 1.6	330 ± 0.3	331 ± 0.3	330 ± 1.8	331 ± 0.2	332 ± 0.1
Dichloromethane	329 ± 1.7	330 ± 0.6	331 ± 0.5	330 ± 1.7	331 ± 0.6	332 ± 0.8
Slowly cooled	301 ± 1.0	307 ± 1.5	313 ± 0.6	302 ± 3.1	314 ± 2.0	324 ± 0.1
Quench cooled	318 ± 0.7	319 ± 0.6	320 ± 0.4	320 ± 0.4	321 ± 0.1	322 ± 0.3

Table S2: T_g and T_g^{mid} of lopinavir raw material, its recrystallisation products and its glasses (mean ± S.D.)

Preparation conditions	T_g (K)			T_g^{mid} (K)		
	5 K/min	10 K/min	20 K/min	5 K/min	10 K/min	20 K/min
Raw material	344 ± 1.1	348 ± 0.4	353 ± 0.5	346 ± 1.0	351 ± 0.5	356 ± 0.3
Ethyl acetate	346 ± 0.4	346 ± 0.7	346 ± 0.6	347 ± 0.5	348 ± 0.2	349 ± 0.3
Acetone	350 ± 0.5	350± 0.1	350 ± 0.4	351 ± 0.7	351 ± 0.2	351 ± 0.2
Diethyl ether	336 ± 0.4	340 ± 2.4	342 ± 2.0	337 ± 0.4	343 ± 3.6	347 ± 3.2
Chloroform	336 ± 0.1	339 ± 2.8	342 ± 1.4	339 ± 0.6	344 ± 0.6	347 ± 0.1
Dichloromethane	327 ± 1.2	331 ± 6.6	336 ± 7.1	329 ± 0.8	336 ± 8.4	343 ± 4.7
Slowly cooled	316 ± 0.6	318 ± 0.1	320 ± 0.2	319 ± 0.1	320 ± 1.6	322 ± 0.1
Quench cooled	350 ± 0.5	351 ± 0.4	353 ± 0.3	351 ± 0.4	354 ± 0.2	357 ± 0.2

Table S3: Corrected relative FTIR peak intensities and ratios (mean ± S.D.)

Preparation medium	Corrected relative intensities			Ratio	
	1650	701	2964	1650:701	1650:2964
Acetone	0.26 ± 0.07	0.21 ± 0.06	0.16 ± 0.02	1.29 ± 0.14	1.68 ± 0.12
Ethyl acetate	0.23 ± 0.02	0.18 ± 0.02	0.15 ± 0.02	1.26 ± 0.14	1.57 ± 0.13
Chloroform	0.39 ± 0.05	0.37 ± 0.05	0.27 ± 0.05	1.05 ± 0.05	1.44 ± 0.08
Diethyl ether	0.15 ± 0.01	0.22 ± 0.01	0.19 ± 0.01	0.77 ± 0.04	0.87 ± 0.06
Dichloromethane	0.02 ± 0.00	0.11 ± 0.02	0.09 ± 0.01	0.24 ± 0.04	0.25 ± 0.04